Food Hydrocolloids 104 (2020) 105751

Contents lists available at ScienceDirect

Food Hydrocolloids

journal homepage: http://www.elsevier.com/locate/foodhyd

β-cyclodextrin- soy soluble polysaccharide based core-shell bionanocomposites hydrogel for vitamin E swelling controlled delivery

Mohamed Eid [a,b,d], Remah Sobhy [a,b,d], Peiyuan Zhou [a,b], Xianling Wei [a,b], Di Wu [a,b], Bin Li [a,b,c,*]

[a] College of Food Science and Technology, Huazhong Agricultural University, 1st Shizishan Road, Wuhan, Hubei, 430070, China
[b] Key Laboratory of Environment Correlative Dietology (Huazhong Agricultural University), Ministry of Education, 1st Shizishan Road, Wuhan, Hubei, 430070, China
[c] Functional Food Engineering & Technology Research Center of Hubei Province, China
[d] Department of Biochemistry, Faculty of Agriculture, Benha University, Moshtohor, 13736, Qaliuobia, Egypt

A B S T R A C T

Hydrogel nanocomposites (HGNCs), with a hydrophobic inner hollows structure and a hydrophilic exterior, is often used to encapsulate the broadest range of guest molecules. Herein, we established a three-dimensional, nanocomposites, superabsorbent, malleable, and bioadhesive HGNCs via chemical crosslinker poly (ethylene glycol) diglycidyl ether (PEGDGE) to enhance the controlled release and bioavailability of Vitamin E (VE). β-cyclodextrin (β-CD) are integrated as multi-core units in the soy soluble polysaccharide (SSPS) polymer network in which the β-CD cavities act as carriers for (VE) by host-guest interaction. We have examined the detailed structures and morphology by FTIR, DSC, XRD, SEM, TEM, AFM, and CLSM. Overall, increasing the β-CD than SSPS in the reaction mixture (from 10 to 25%) led to enhance the crosslinking degree, improve the elastic behavior ($G'>G''$), increase the particle size (from 114.2 to 202.9 nm), and the hardness. Besides, decreasing the adhesiveness, pore size, and swelling. Our (HGNCs) did not rupture under compression up to 90% strain with (1.8 MPa) strength. The nanocomposites (1:1) exhibited less nanosized after pectinase and α-amylase hydrolysis (75 and 124 nm, respectively). Also, the (HGNCs) exhibited outstanding swelling-adsorption and sustained release (over 230 h) towards VE in vitro. It showed high encapsulation efficiency and loading capacity (79.10 and 16.04%, respectively). Additionally, the oral administration of VE-loaded HGNCs in rats resulted in a sustained increase of plasma VE levels over 12 h post-administration. The relative pharmacological bioavailability of VE was larger for VE-loaded HGNCs (reached to 7.5-fold increase) compared to free VE suspension. **Keywords**: Nanohydrogel; β-cyclodextrin; Soy soluble polysaccharide; Vitamin E; swelling; control release.

1. Introduction

Nanocomposites (NCs) can be classified into several classes, and one highly skillful type is the NCs based on biopolymeric hydrogels (Hussain & Mishra, 2018). Hydrogel nanocomposites (HGNCs) has shown interesting suitable properties that play an essential role among drug delivery vectors. The enhancement of HGNCs that deliver vitamins, antioxidants, drugs, and dyes is a great strategy (Kaur & Jindal, 2019; Olad, Doustdar, & Gharekhani, 2018). Thus, a perfect design of the HGNCs would improve the incorporation of a large quantity of drugs, especially the hydrophobic one, with efficient and prolong release. The HGNCs has unique properties because it combines the characteristics of typical hydrogels, besides the features of nanoparticles (NPs), such as high and reactive surface area, which can significantly enhance the absorption capability in vitro and in vivo (Becher et al., 2018). Many hypothesis tried to solve the problems of the short term release and fast diffusion like microcapsules (Jiang et al., 2019), films (Zhu, Lee, & Yam, 2012), and electrospun bioactive glass hollow fibers, due to the coarse surface and tubular structure (Wu et al., 2011). Swelling controlled-release hydrogel (SCRH) is an innovative smart technology by which bioactive composites released in a low emotion but controlled way (Li et al., 2015; Shi, Xiong, Liu, Wang, & Zhao, 2016). swelling with pH-responsive is mostly important for oral and tumor delivery systems. In this application, the swelling of the hydrogels in the acidic media (stomach) is minor, and thus the drug is still entrapped and protected. As the hydrogels reached the intestinal tract anywhere the pH is neutral, and the network can be swell dramatically, permitting for quick drug diffusion (Mumper, Huffman, Puolakkainen, Bouchard, & Gombotz, 1994). Such hydrogels have been industrialized using polymers with acidic functional groups; between them, the alginate (most commonly used) and the SSPS as a promising polymer used in this study.

Many studies provided details of the chemical composition and physical properties of the SSPS as a biopolymer. However, they have not yet made enough improvement in its applications. A few research groups focused on SSPS as a shell material for bioactive ingredient delivery systems. For examples (Ding & Yao, 2013), formed the soy protein/SSPS complex as nanogel by high pressure homogenization (600 bar) followed by heat treatment (90 °C) under acidic conditions to control

* Corresponding author. College of Food Science and Technology, Huazhong Agricultural University, 1st Shizishan Road, Wuhan, Hubei, 430070, China.
E-mail address: libinfood@mail.hzau.edu.cn (B. Li).

https://doi.org/10.1016/j.foodhyd.2020.105751
Received 7 August 2019; Received in revised form 29 January 2020; Accepted 6 February 2020
Available online 8 February 2020
0268-005X/

release of folic acid (FA) in PBS (pH 7.4) at 37 °C. Then, the results demonstrated a quick release for both free and encapsulated (FA). It was also described that SSPS can be used to form core-shell with soy protein nanoparticles as carriers for further sustained-release behavior of encapsulated curcumin (F.-P. Chen, Ou, & Tang, 2016). Chen et al. treated the SSPS with ethanol (40% v/v) under acidic conditions (pH 4) to denature the protein fraction of SSPS to interact with curcumin by a hydrophobic interaction with encapsulation efficiency (67.3%) and loading amount (4.49 μg/mg SSPS) (F. P. Chen, Ou, Chen, & Tang, 2017). It was also found that the SSPS with low protein content (<5%) can be used to produce more degradable films than high protein content (mostly used as potential emulsifier) (D. Salarbashi, Bazeli, & Tafaghodi, 2019). Furthermore, the SSPS is a highly branched globular shape (Hosny, Mosli, & Hassan, 2015), and this characteristic enables the particles to interact efficiently with cells with significant uptake, which may enhance the bioavailability of drugs (Chithrani, Ghazani, & Chan, 2006; Lu, Zhao, Wu, Zhao, & Yang, 2019). On the other hand, the SSPS has some weakness such as low viscosity, and small mechanical properties, which can limit its uses in the industrial fields. Besides, it can interfere with the protein-protein interactions in wet conditions so it favorable to complex with saccharides (D. Salarbashi et al., 2019). Therefore, a promising area is to utilize the SSPS-based adhesive HGNCs with other polysaccharides or oligosaccharides to add some mechanical, rheological, and biological properties in food industry and pharmaceutical applications.

This restriction of the SSPS-based HGNCs can be solved by formulating β-cyclodextrin (β-CD, 7- α-D-glucopyranose units) imbedded SSPS-based HGNCs. Additionally, this formula with β-CD can improve the inclusion complex (IC), stabilize the hydrophobic drugs, prevent drug/drug interactions, enhance the mechanical and rheological properites (Yuan, Xu, Cui, & Wang, 2019), increase the bioavailability, convert oils and liquid drugs into amorphous powders or microcrystalline, increase the loading and control release. Besides, it has been recognized as a flavor carrier and preserver, at a level of 2% in several foodstuffs. Neverthless, the β-CD has some disadvantages like limited water solubility resulting in precipitation of solid β-CD complexes from water, besides cannot be hydrolyzed by human salivary and pancreatic amylases. It can be fermented by the intestinal microflora (colon), (Hedges, 2009). Many ideas tried to increase the SSPS applications by using different materials like (Nano-clay Na^{+}, Zinc oxide, Titanium dioxide), but there are growing concern has elevated over the health risk of these NPs following possible transition into human foods. Which, should be evaluated before the massive applications in food (Davoud Salarbashi, Tafaghodi, & Bazzaz, 2018; Shaili, Abdorreza, & Fariborz, 2015). On the other hand, Vitamin E (VE) exhibits poor aqueous solubility and a high sensitivity to oxidation, resulting in loss of bioactivity. More especially, the best absorption site of VE is the small intestine. Therefore, developing a delivery system for encapsulating VE to develop its release, stability, and bioavailability is required. Various formulations have been demostrated to enhance the controlled release and bioavailability of VE. For example, polymeric electrospun nanofibers incorporating β-CD has been used to host several bioactive compounds like VE but with limited loading capacity up to 5% (w/w). Besides, it has some drawbacks like fast diffusion and no mechanical or rheological properties (Z. Aytac, Kusku, Durgun, & Uyar, 2016; Celebioglu & Uyar, 2017). Also, Cassano et al. determined the release rate of VE by using dextran -ferulic acid as swelling hydrogel polymers and noted that the released reached 65% in 24 h with less than 15% VE-loaded (Cassano, Trombino, Muzzalupo, Tavano, & Picci, 2009).

This study formulated elastic, bioadhesive, biodegradable, eco-friendly, and swollen HGNCs containing β-CD and SSPS as multi-core-shell nanocomposites, respectively based on the chemical cross-link. These ingredients were characterized by FTIR, DSC, XRD, SEM, TEM, AFM, and CLSM to recognize the structure-properties linking and how these two polymers could modify the adhesiveness, mechanical, rheological, and release properties of the HGNCs in vitro and in vivo (oral bioavailability). The β-CD core can be used to encapsulate the VE as water-insoluble drug (host-guest interaction) using the (SCRH) technique. While, the hydrophilic SSPS shell can be used to enhance the bioavailability, dispersibility, and impart functional characteristics to the HGNCs surface. In brief, the swelling and VE release rate increased with the quantity of SSPS than β-CD incorporated. Considerable research has performed on copolymer-based hydrogels, but no specific work has been done until now to characterize β-CD/SSPS together as HGNCs. Hopefully encouraging their applications as functional biomedical materials.

2. Materials and methods

2.1. Materials

β-cyclodextrin (≥97%, molecular weight (MW) 1134.98 g/mol, was dried at 80 °C over three days before use, Sigma Aldrich, USA). Soy soluble polysaccharides obtained from Shanghai yuan ye Biotechnology Co., Ltd., purity ≥95%, galacturonic acid 18% (w/w), protein 3.05%, Moisture 0.5%, Ash 1.45%, and as reported before that the main backbone of SSPS contains (homogalacturonan and rhamnogalacturonan with branches of α-1,4-galactan and α-1,3- or α-1,5-arabinan chains) (Nakamura, Furuta, Maeda, Takao, & Nagamatsu, 2002). PEGDGE (cross-linker; poly (ethylene glycol) diglycidyl ether, Mn 500 g/mol, Aldrich). (+)-α-Tocopherol (VE) from vegetable oil, Type V, ~1000 IU/g, Sigma Aldrich, USA). 1-anilinonaphthalene-8-sulfonic (ANS) from Aladdin-reagent Co., Ltd. (Shanghai, China). Pectinase (30,000 U/g, from Aladdin company, Shanghai, China) and α-amylase from porcine pancreas type VI- B (enzyme activity ≥ 10 units/mg solid, Sigma-Aldrich). The water used from a Millipore Milli-Q ultrapure water system.

2.2. HGNCs formation

In this study, four types of HGNCs (β-CD/SSPS) formed by suspension chemical crosslinking. A typical procedure to prepare the hydrogels is as follows: SSPS (20%, w/v) and 10, 15, 20, and 25% of β-CD were dissolved in 1.5 mol L^{-1} aqueous Sodium hydroxide solution (NaOH, 10 mL) and left-over night for full hydration in 25 mL glass tubes. Next, 1.075 g (2.15 mmol) of PEGDGE added dropwise to the solution under stirring at 25 °C for mixing. After that, the tubes were incubated at 60 °C for 4 h under 300 rpm. The resulting hydrogels were further immersed into enough deionized water and ethanol solution (1:1, v/v) for four days under shaking to reach the swelling equilibrium and until residual and unreacted materials wholly removed. Phenolphthalein dye used to notice the excess of NaOH removal inside the washing solution until it became colorless. The SSPS tested only as a reference, but not formed the expected gel. Finally, all the swelling hydrogels dried at 40 °C under reduced pressure and stored in a desiccator until use. The mass ratio between the two polymers (β-CD: SSPS), were varied to depict the effect of hydrogel compositions on its properties. The (β-CD: SSPS) ratio was fixed at 1:1 for some studies. The complexation of VE by native β-CD was performed according to the method of Koontz et al. (Koontz, Marcy, O'Keefe, & Duncan, 2009).

2.3. FTIR spectra measurements

The infrared spectra of the pure VE, β- CD, SSPS, and HGNCs, besides the β- CD/VE- IC, and HGNCs/VE complexes were obtained via a Fourier transform infrared spectrometer (FTIR) by a Nicolet 470 (Thermo Fisher Scientific, USA). The samples arranged as pellets by compressing with the background Potassium bromide (KBr) for the analysis. The scans (21 min^{-1}) recorded between 4000 and 400 cm^{-1} with a resolution of 2 cm^{-1} and The Omnic software obtained the spectra baselines.

2.4. X-ray diffraction (XRD)

The examination was set by using D/max-RA, Rigaku, Tokyo, Japan (30 mA and 50 kV), Using Cu target and Kα (λ = 1.54 Å), Ni filter, and radiation at room temperature. All scans performed in a 2θ range of 3–40 at step size 0.02 s^{-1} with scanning speed 10°/min. The analysis was conducted only for all the solid powder samples except for VE (Liquid form at room temperature).

2.5. Differential scanning calorimetry (DSC)

DSC and transition glass (T_g) performed on (DSC200F3, NETZSCH instrument, Germany) with 5 mg same samples. For dehydration and vaporization, our samples heated from 25 to 250 °C at a rate of 10 °C/min under N_2 atmosphere (flow rate 30 mL/min). For the transition glass (T_g) samples were equilibrated at −90 °C and then heated to 25 °C at a heating rate of 10 °C/min.

2.6. Scanning electron microscopy (SEM) analysis

SEM apparatus Hitachi X-650 (Hitachi Ltd., Japan) was used to examine the microstructure of the hydrogel slices surface by using the razor to prepare samples. The water-swollen samples at 25 °C for 48hr in water used flash-frozen by liquid nitrogen for 3 min and rapidly lyophilized for 48 h. The samples immobile on aluminum stubs by using double-phase tape then covered with gold by using a microscope sputter coater Au–Pd (SC7620, UK). All samples examined under the accelerating of 20 kV voltage.

2.7. Transmission electron microscopy (TEM) and atomic force microscopy (AFM)

Hitachi-7650 transmission electron microscope (Hitachi Ltd., Japan) operating at 110 kV. TEM samples were prepared by dropping 10 μl of (0.5 mg/mL) hydrogel dispersions onto carbon-coated copper grids and dried at room temperature for 24 h. However, the 2-D and 3-D morphology of the HGNCs (1/1) were characterized by atomic force microscopy (AFM) (Bruker Dimension Icon Nanoscope V, Germany). Briefly, freeze-dried HGNCs were diluted with water to obtain HGNCs concentration of 0.5 mg/mL. After dispersion by using ultrasonic, the solution (about 10 μL) was adsorbed onto a piece of freshly cleaved mica sheet and dried at 25 °C for 12 h before imaging. The imaging was conducted in a tapping mode with a scan rate of 0.5 Hz at room temperature.

2.8. Rheological measurements

The rheological analysis of the swelled hydrogels was evaluated in triplicate and carried out at 25 °C on a Discovery HR-2 Hybrid Rheometer machine (TA Instruments, USA) attached with parallel geometry sensor (60 mm diameter, Peltier plate Aluminum, and gap height 1 mm). The oscillatory rheological analysis was done in the linear viscoelastic regime. The strain was kept at 0.1%, and a dynamic frequency sweep started from 0.1 to 10 rad/s to measure the elastic modulus (G′), and viscous modulus (G″). The shear viscosity was considered by measuring flow curves recorded at shear rates from 2 to 200 s^{-1}. Also, the influence of time on viscosity observed from (35- 700 s^{-1}).

2.9. Mechanical properties

Compression and loading-unloading tests were performed at 25 °C by using CT3-Texture analyzer (Brookfield, Middleboro, MA). The hydrogel samples prepared as a cylinder shape with a height of 15 mm and diameter 20 mm (The diameter of the hydrogel was measured with a caliper (Digimatic Caliper, Liangju Co. Ltd., China). The compression rate was done at 20% min^{-1} strain rate with a constant velocity of 5 mm min^{-1}. For the loading-unloading test, the compression rate was kept at a strain rate of 20% min^{-1} to measure the hardness, adhesiveness, and the elastic modulus (Young's modulus), which considered from the slope stress-strain curve. The high flexibility confirmed by the compression at 90% strain with five loading/unloading cycles.

2.10. Swelling behavior

Hydrogel samples were prepared to investigate the properties of the swelling equilibrium in water. 100 mg sample was soaked at 25 °C for 24 h, and the equilibrium ratio of the swelling is calculated as follows:

$$(\textbf{Equilibrium swelling ratio}\ ,\ \%) = \frac{W(s)\ -\ W(d)}{W(d)}\ \times\ 100 \quad (1)$$

where W(s) and W(d) is the calculated weights of the swollen and dried samples, respectively.

2.11. Dynamic light scattering (DLS), ζ- potential and surface hydrophobicity (H0) measurements

The DLS and ζ- Potential were achieved on (Zetasizer Nano ZS series, Malvern Instruments, UK) at 25 °C. The DLS measurements were done with a scattering angle of 173°, and the apparent (Z-average) hydrodynamic diameter (D_h) was reported as the intensity. We used the native β-CD and SSPS solutions, besides the dispersions of the HGNCs freeze-dried samples with and without VE at a concentration of 0.1% (w/v) aqueous solution. The ζ potential was determined with the SSPS and HGNCs (1/1) with and without VE aqueous dispersion solutions, the ζ potential samples were prepared by adjusting the stock solutions to the chosen pH values and then separately diluted to 1 mg/mL for HGNCs and 5 mg/mL for SSPS with the same pH value. For the (H0) analysis, samples were measured using 8-anilino-1-naphthalene sulfonic acid (ANS) as a fluorescence probe (Alizadeh-Pasdar & Li-Chan, 2000; Xiong et al., 2016). The ANS solution obtained by preparing 8 mM of ANS powder in 10 mM phosphate buffer (PB). Moreover, 25 μL of 8 mM ANS was added to 5 mL sample solutions which contain 1 mg/mL dispersed samples. After keeping away from light for 8 min at 25 °C, the fluorescence intensities of ANS/(HGNCs) and (HGNCs/VE) dispersions were recorded using a fluorescence spectrophotometer (Shimadzu RF-5310PC, Japan). The excitation wavelength was 390 nm, and the emission spectrum were taken between 400 and 650 nm. The excitation and emission slit widths were both 5 nm, with 700 V, and the scan speed was 1200 nm/min. The area of the fluorescence spectrum corrected by taking the solvent area, and (H0) expressed as the sample area.

2.12. HGNCs polysaccharide enzyme hydrolysis (pectinase and α-amylase)

We also confirmed the core-shell structure by using enzymes as follows: the SSPS on the freeze-dried HGNCs surface was hydrolyzed by pectinase. So, for tracking the size change by real-time DLS measurement, the hydrolysis was performed at pH 4.0 and 25 °C. And to achieve the DLS measurement, 10 μL of 0.1% (30 units/ml) pectinase enzyme solution was added to a polystyrene cuvette containing 0.5 mg/mL of the HGNCs dispersion. The solution diluted with 5 mL of pH 4.0 aqueous solution, and the size was measured every 10 min (Ding et al., 2013). The β-CD on the HGNCs was hydrolyzed by α- Amylase and for monitoring the size change by real-time DLS measurement, the hydrolysis was performed at pH 7.0 and 25 °C. Also, to do the DLS measurement, 10 μL of 0.1% (16 units/ml) α- Amylase solution was added to a polystyrene cuvette containing 0.5 mg/mL HGNCs dispersion. The solution diluted with 5 mL of pH 7.0 aqueous solution, and the size was measured every 10 min (Y. Wang, Luo, et al., 2018).

2.13. Confocal laser scanning microscopy (CLSM)

Nile Blue and Nile Red solutions (0.1 mg/mL) were prepared using deionized water and ethanol as solvents, respectively. A total of 0.005 g of β-CD/VE- IC and HGNCs/VE were immersed in 20 μL of Nile Blue and 20 μL of Nile Red solutions and kept in the dark overnight (P.-P. Wang, Luo, & Peng, 2018). The sample slide was prepared and measured at the excitation wavelengths of 488 and 633 nm by CLSM (Olympus FV1200, Japan), respectively.

2.14. In vitro VE complexation and dynamic release by swelling technique

The abilities of the HGNCs to host VE as a guest molecule by swelling was estimated by the following procedure: each hydrogel sample (100 mg) was placed into 25 mL pure water containing VE ethanol solution (25%, w/w) at a 50-mL tube. After the addition of VE, a stable white and cloudy dispersion was formed (emulsion form). Next, the tubes were capped and placed in a shaker under 150 rpm oscillation at 25 °C, and after 48 h the hydrogel samples were out from the solution and washed with water/ethanol (1/1) to remove the VE from the hydrogel surface. Then, the hydrogels were crashed by spatula and sonicated in the presence of absolute ethanol. The tubes were left under magnetic stirrer for another 48 h to be sure that all the complexed VE extracted by the pure ethanol. Finally, the extract was filtrated and measured on UV–Visible spectrophotometer (UV-1700, Shimadzu, Japan) at 295 nm. The concentrations of VE were determined by using a calibration curve. The added of VE concentration was estimated from the highest weight β-CD content inside the hydrogel by using theoretical conversion of a 1:1 ratio of β-CD and VE. The complexation efficiency (CE) of each hydrogel and loading capacity (LC) toward VE were calculated by these Eqs. (2) and (3).

$$(\mathbf{CE},\ \%) = \frac{\text{Complexed VE inside the hydrogel}}{\text{The total amount of VE}} \times 100 \quad (2)$$

$$(\mathbf{LC},\%) = \frac{\text{Complexed VE inside the hydrogel}}{\text{Total weight of the hydrogel}} \times 100 \quad (3)$$

While, the release rate of VE from the HGNCs was evaluated by using a 0.05 M phosphate buffer saline (PBS) solution at pH 7.4. In order to improve the solubility of the unrestricted VE in aqueous media, the release solution contained Tween-20 (0.5% w/v) (Butt et al., 2019; X.; Chen, Lee, Zhu, & Yam, 2012). 100 mg of dried (HGNCs/VE) samples were incubated in the release media at 25 °C under shaking with a speed of 150 rpm. The hydrogels swelled up and turned from the glassy state to rubbery state, and at the scheduled time, 1 mL was withdrawn from the release media and replaced with another 1 mL fresh buffer solution. Cumulative VE released was measured using UV- absorbance measurement at 295 nm. We used the hydrogels without VE and the release buffer as a control and blank, respectively. It should be noted that the in vitro model cannot precisely simulate the complex processes happening within a living gastrointestinal tract, but it is suitable for speedily screening diverse samples and for identifying chief physicochemical mechanisms.

2.15. In vivo VE bioavailability and pharmacokinetics study in rats

A total of thirty-six SPF Albino Westar rats weighing approximately (200–220 g) were purchased from Wanqian Jiaxing Biotechnology Co., Ltd (Wuhan, China). The rats were housed in cages under a 12 h light/dark cycle at 22 ± 1 °C and 55% relative humidity. All experimental performance was following the National Institutes of Health guide for the care and use of laboratory animals (NIH Publications No. 8023, revised 1978), and supervised by (Huazhong Agricultural University Ethics Committee of Care and Use of Laboratory Animals). After one-week acclimatization, the rats were randomly assigned into six following groups (6 rats per group): the control group with only HGNCs without VE (labeled as "Control"), the free Vitamin E (25%, w/w) with 2% (Tween 20) group (labeled as "free VE suspension"), the HGNCs/VE complex groups (labeled as "(10/20), (15/20), (20/20), and (25/20) %, respectively"). Before the experiment, the animals were fasted (16 h) with water *ad libitum*. In the next early morning, the rats of each treated group were oral administered. The same dose (100 mg) of HGNCs or HGNCs/VE was ensured for each rat with 3 mL water. At zero time and subsequent each hour interval until 24h, 200 μl of a blood sample from each rat was collected from the tail vein and placed into heparin sodium anticoagulant tubes. Next, the plasma was separated from the whole blood by centrifugation at 4000 rpm for 10 min and stored at −80 °C until further analysis. The concentration of plasma VE was analyzed using plasma VE assay kit (colorimetric method) (Nanjing Jiancheng Biological Engineering Institute Co. Ltd; China). A washout period of one week between two successive experimental administrations was allowed to remove any effect of the prior dose. The pharmacokinetics parameters like maximum plasma concentration (C_{max}), the time of maximum plasma concentration (T_{max}), elimination rate constant (K_e), and area under the curve ($AUC_{0\text{-}t}$ and $AUC_{0\text{-}\infty}$) were determined (Zhang, Huo, Zhou, & Xie, 2010). The percent relative bioavailability (BA, %) was also calculated by using this formula:

$$(\mathbf{BA},\ \%) = \frac{\text{AUC (HGNCs/VE)complex}}{\text{AUC (free VE suspension)}} \times 100 \quad (4)$$

2.16. Statistical analysis

Measurements performed on three or more samples, and the results are given as means ± standard deviations, using the statistical software SPSS (SPSS Inc., Chicago, IL, USA).

3. Results and discussion

Poly (ethylene glycol) diglycidyl ether (PEGDGE) can be used to fabricate a biodegradable, soft, stretchable, and tough hydrogels with smart swelling properties (Salvekar et al., 2017). On the other hand, recently some studies showed that using PEG low molecular weight (400–1000 g/mol) had well interaction with nanopolymers and nano-fillers than high molecular weight, which improved the flexibility of the materials (Faradilla, Lee, Sivakumar, Stenzel, & Arcot, 2019). Besides, it can quickly be degraded and released from the body after taken (Jokerst, Lobovkina, Zare, & Gambhir, 2011; Zhao et al., 2019). The PEGDGE used as reactive polymeric cross-linker for β-CD and SSPS in aqueous strong alkaline media (Fig. 1), the PEGDGE have the ability to crosslink between the hydroxyl and amine groups that further react between the polymers group, and this process leads to the formation of a three-dimensional polymer network and may be used for the preparation of different hydrogels (Kono, Onishi, & Nakamura, 2013), the biopolymers possess nucleophilic attack between the two equivalents of an alkoxy anionic polysaccharide species, which is created under basic circumstances to form the ether cross-linkage (Rodriguez, Alvarez-Lorenzo, & Concheiro, 2003). With this reaction, HGNCs prepared by simple preparation method in an aqueous solution without VE. This chemical reaction strongly depends on the reaction parameters.

3.1. The FTIR analysis

The (Fig. 2a) showed the Infrared-spectroscopy of lyophilized purified HGNCs different ratios. It was noted that by increasing the β-CD content inside the reaction mixture, some bands appeared with increasing intensity like (3400, 2919, 1643, 1106, and 1033 cm^{-1}), respectively as ordered in the figure. To confirm the HGNCs formation, the absence of the band at 1106 cm^{-1} in the β-CD IR-spectrum (Fig. 2b), and presence in the HGNCs confirm the chemical cross-linking between the two biopolymers, which related to the single bond stretches like (C–C (SP^3), C–O, and C–N), besides the (1033 cm^{-1}) band represent the

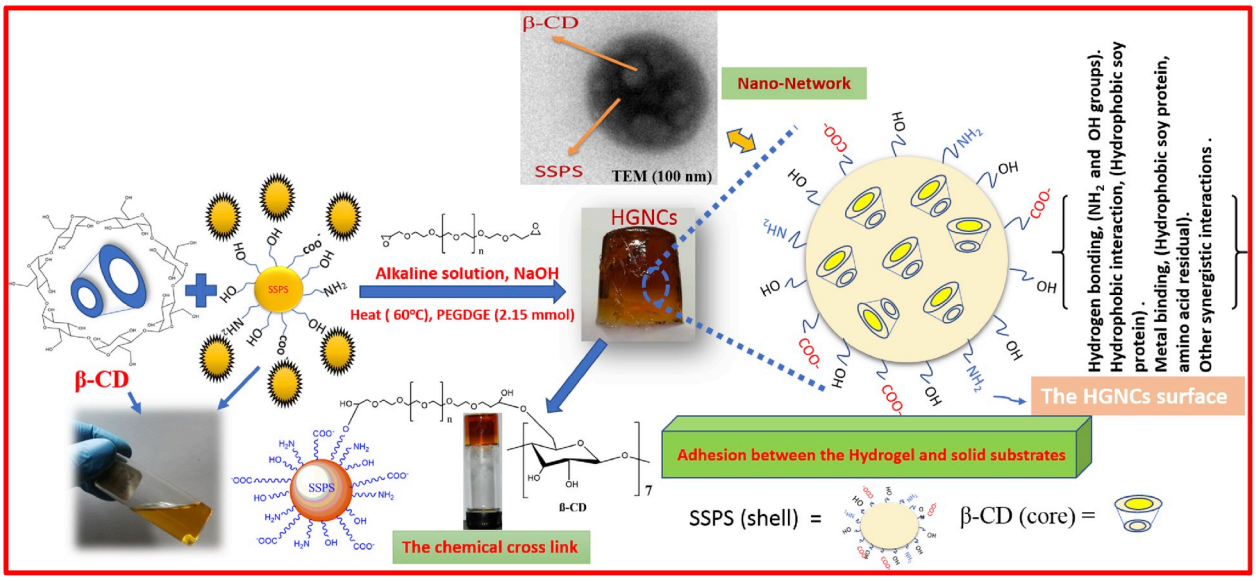

Fig. 1. Schematic illustration of the HGNCs formation with the adhesiveness property.

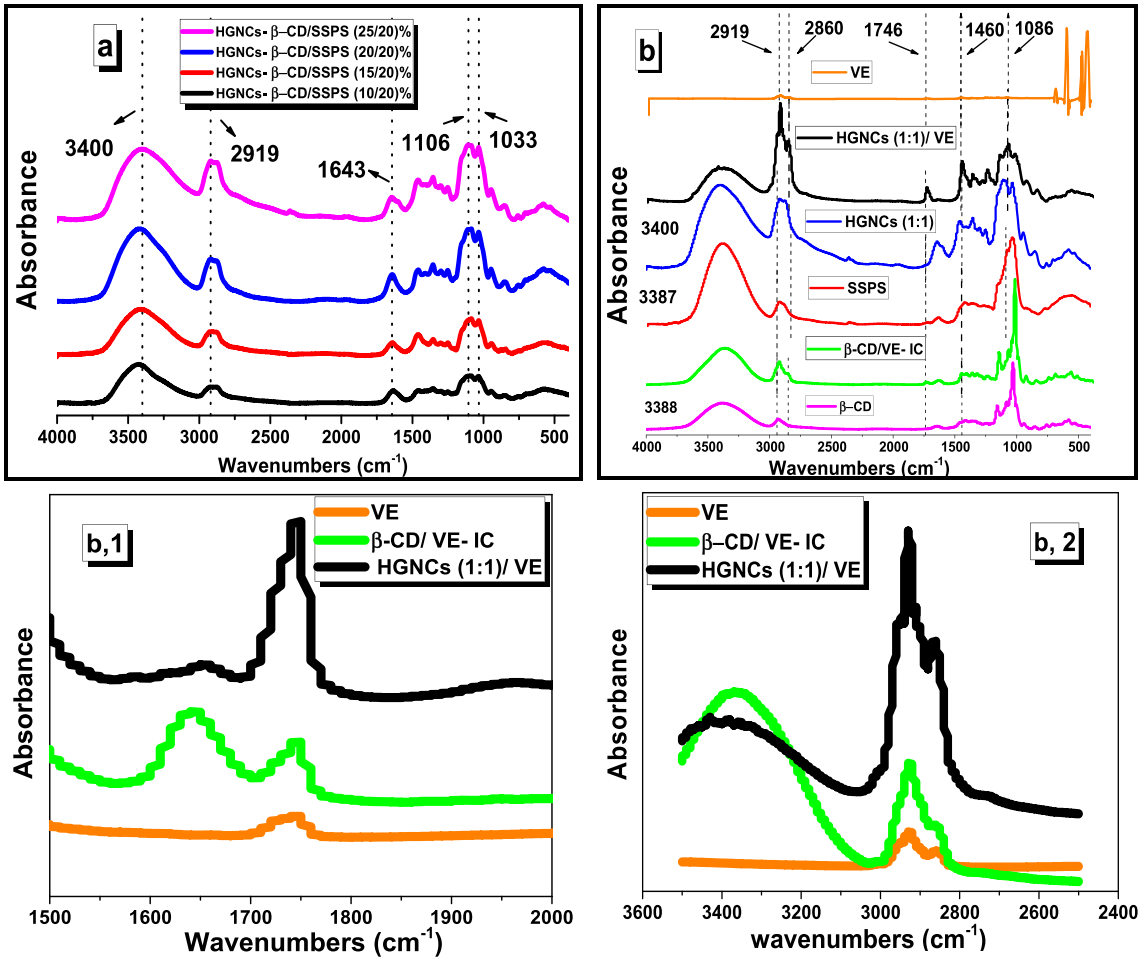

Fig. 2. **(a)** FTIR-spectra of HGNCs with increasing β-CD content **(b)** FTIR-spectra of β-CD, pure VE, β-CD/VE –IC and HGNCs/VE complex in full range (4000-500 cm-1) **(b,1 and b,2) showed the** expanded range from fig. b (1500–2000 and 3600-2400 cm-1). The ratio of β-CD: SSPS fixed at (1:1).

stretching vibration of C–O–C bond (Fig. 2a). Analyses of β-CD, VE and β-CD/VE-IC were carried out to investigate the presence of VE in the HGNCs samples besides the SSPS as a copolymer inside the gel (Fig. 2b). For β-CD/VE-IC and HGNCs/VE complexes, the characteristic absorption peaks noticed at around 1029, 1055, 1081, 1156, 1243, 1366, 1414, 1644, 2929, and 3388 cm−1 are related to the single bond stretching

vibration (C–C) and asymmetric C–O, asymmetric stretching vibration of the glycosidic bond C–O–C and alkyl aryl ether R-O-R, H–OH bending (alcohol, carboxylic acid, amine group N–H, water adsorption, C–H stretching vibrations, and O–H stretching vibrations, respectively. The characteristic peaks of VE has shown at 1086 cm^{-1} assigned for stretching vibration of sp^3 C–O in the heterocyclic benzene, 1460 cm^{-1} due to C=C stretches in the aromatic ring and for the symmetrical methyl bending, 2860 and 2926 cm^{-1} corresponded to symmetric and asymmetric stretching of aliphatic hydrocarbon sp^2 and sp^3 C–H groups, respectively. With addition of the VE, a slight decrease in the absorbance intensity and the area under the peak detected; this can be attributed to the Host-Guest interaction, which causes covering the (-OH) groups like 1643 cm^{-1} with the HGNCs/VE complex and shifted to be 1746 cm^{-1} which noted with β-CD/VE-IC and HGNCs/VE complex, besides increasing the intensity at 2919 cm^{-1} band which related to the (-CH alkane groups) like C–H vibrations, C–H groups, C–C, and all these groups formed the glucopyranose ring of the β-CD and VE, which observed in the complexation. The characteristic peaks of VE presence inside the β-CD-IC and HGNCs/VE complex in some regions like (1746, and 2860 cm^{-1}) were magnified in (Fig. 2b1 and b2), and it is noticeable that the intensity increased with the addition of VE. In conclusion, these results confirmed the IC.

3.2. XRD studies

XRD is a useful technique for the recognition of cyclodextrin complexation in powder or microcrystalline states (Michalska et al., 2017). It has been reported that the appearance of new peaks and disappearance of characteristic peaks are all evidence of the formation of (IC) (Celebioglu et al., 2017; Trindade et al., 2019). As indicated in (Fig. S1).

3.3. DSC analysis

DSC is a fast and dependable technique to prove the (IC) between the guest molecules and host CDs (Celebioglu et al., 2017; L. X. Song, Bai, Xu, He, & Pan, 2009; Trindade et al., 2019). For example, the absence of thermal transitions such as glass transition temperature (T_g) of a guest molecule in a CD-IC is generally taken as evidence of the proper (IC). In DSC thermogram of the pure VE, we can notice that the (T_g) around −58.3 °C, which corresponds to the transition from glassy state to a supercooled liquid (Fig. 3b) (Koontz et al., 2009). On the other hand, there is no Tg recorded for VE in the case of β-CD-IC and the HGNCs/VE complex suggesting that the VE in the β-CD and HGNCs matrix absolutely complexed within the β-CD cavity (Zeynep Aytac & Uyar, 2017; Celebioglu et al., 2017). Also, the total enthalpy change (ΔH in J/g) formed in the DSC thermograms is due to the dehydration of β-CD molecules, and the ΔH differences between pure β-CD and β-CD/VE-IC can demonstrate the complex formation (Veiga, Merino, Fernandez, & Lozano, 2002). As it is known, guest molecules compete with water molecule which exists in the β-CD cavity during the complexation. Therefore, ΔH value obtained as a replacement of water molecules will be lower in (IC) with the β-CD and HGNCs structure compared to pure β-CD. Here, the ΔH and peak temperature were determined in the range of 25–250 °C for the samples by performing the calculation using the NETZSCH- Instruments Software program as presented in (Fig. 3a). The ΔH values were calculated as (249.5, 187.8, −27.58, 17.42, 28.97, and −5.88 J/g), and the peak temperature values were determined as (189.0, 160.0,174.0, 122.1, 90.1, and 176.0 °C) for β-CD, β-CD/VE-IC, pure VE, SSPS, HGNCs, and HGNCs/VE complex, respectively. Finally, the apparent decrease in ΔH value and different peak temperatures supported also the (IC) formation.

3.4. Morphology study (SEM)

The SEM showed the surface morphology of the HGNCs in (Fig. 4). Our HGNCs exhibited a uniform three-dimensional (3D) network structure. The pore size of the HGNCs was much bigger when its β-CD addition was 10%, while the HGNCs whose β-CD addition was 25% showed the smallest pore size with condensing. Results got from swelling can approve the SEM image very well. We attributed the higher swelling and bigger pore size of HGNCs (10/20)% is due to the higher weight ratio of SSPS in aqueous solutions (Chivero, Gohtani, Ikeda, & Nakamura, 2014), and that is why our HGNCs with a higher amount of

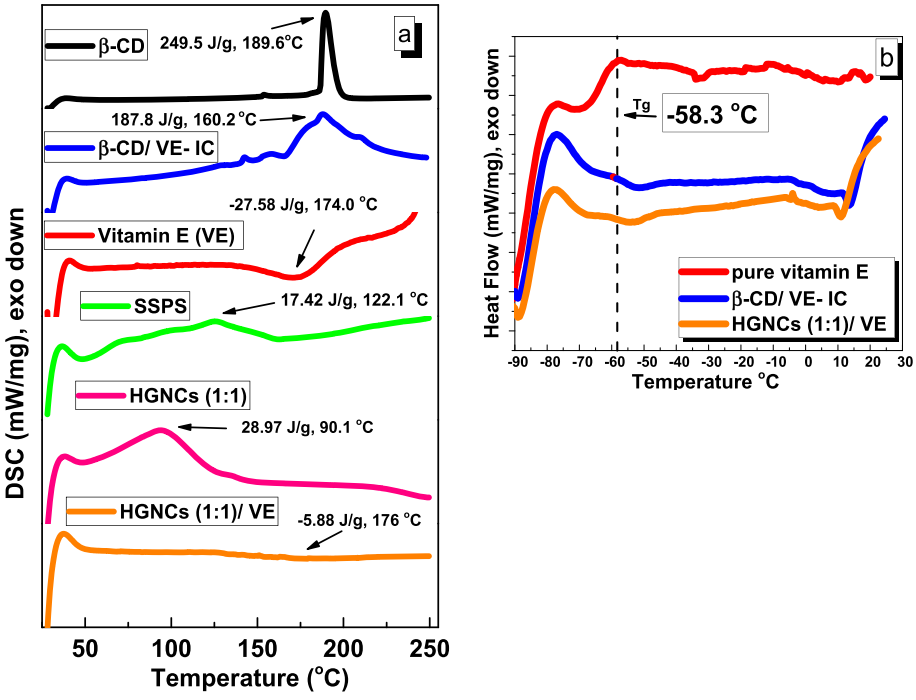

Fig. 3. DSC thermograms of β-CD, pure Vitamin E, β-CD/Vitamin E –IC and HGNCs/VE in a temperature range (25–250 °C) **(a)** and Transition glass (Tg) from (-90-25 °C) **(b).**

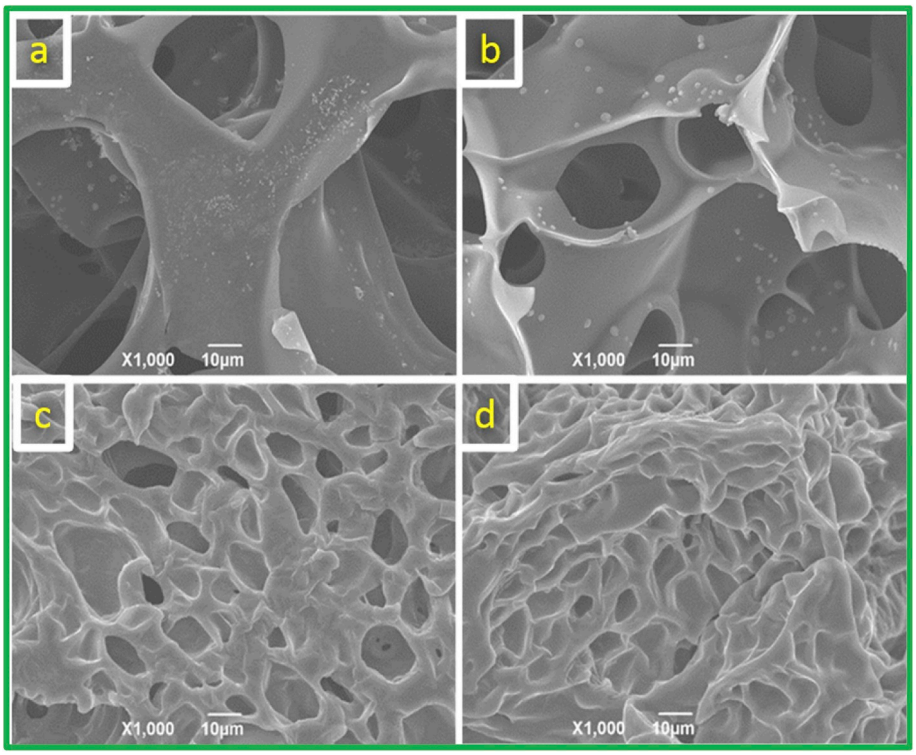

Fig. 4. (a–d) SEM images of different lyophilized HGNCs quenched with liquid nitrogen: (a–d) HGNCs formed from the weight ratio (10/20), (15/20), (20/20), (25/20) % (β-CD/SSPS), respectively in aqueous solution.

SSPS got less strength and low mechanical properties but having a good adhesiveness than others. The SEM reveals that the pore size of the 20% and 25% β-CD were decreased in comparison to the 10% and 15%, which leads to the enhancement of the mechanical properties and supported the slow-release properties. The images exhibited that the HGNCs equipped with an open and interconnected porous structure because of the loss of water during the freeze-drying process. Also, the significant differences in the thickness, smoothness, and roughness of the pore walls were observed, which indicate that the combination with the SSPS had a significant effect on the microstructure.

3.5. TEM and AFM analysis

The TEM imaging was used to further study the size distribution and morphology of the obtained HGNCs (Fig. 5a). The TEM images showed spherical nanoparticles (SNPs) with homogeneous and uniform size distribution. The average size of the SNPs observed in the TEM different than DLS measures (≈53 nm difference). The TEM images of HGNCs (1/1) in the dry state prepared in 0.1 wt % aqueous dispersion reveals uniform particle morphology with a mean size of (D_h,120.4 ± 21 nm) and polydispersity index (17.98%) as analyzed by using Gaussian fitting with size distributions (Fig. 5c). All the particles ranged from 48.4 nm as a minimum size and 173.4 nm as a maximum size from the total sum around 72 NPs appeared in the TEM image (Fig. 5a). On the other hand, the size on wet state increased to an average diameter of 174.3 ± 3 nm, as mentioned in the DLS section. The intended volumetric (de)-swelling ratio defined as (D_h dry/D_h swollen)^3, while the (D_h dry = hydrodynamic diameter under dry conditions, and D_h swollen = hydrodynamic diameter for extremely swollen HGNCs in water) with averages 0.329 (Saunders & Vincent, 1999). Thus, the HGNCs exhibit outstanding swelling properties in water up to more than one time (1.4) than their original size (Fig. 5 b). showed that all the SNPs related to (HGNCs/VE) were formed with a dark black central part, which suggested that the VE sited in the HGNCs core compared with the HGNCs without VE, and this also confirmed by CLSM pictures. The nanosized of the (HGNCs/VE) particles was found to be 123.4 ± 11.8 nm, but this results also opposite to the DLS measurements (245 ± 6 nm), which can be attributed to the fact that this technique measures the NPs in a dry state under the TEM vacuum (dehydrated form), while the DLS measures them in an aqueous environment and confirmed that our HGNCs can absorb much water and swollen (Fig. 5 d and e). represents the 2- and 3-D AFM images of the HGNCs (1/1), which confirmed that the HGNCs are dispersible and spherical nanoparticles. The thickness and the size of the HGNCs were found to be (3.4 and 122 nm), respectively, which confirmed the TEM results and indicates the formation of the HGNCs. Besides, from the TEM and AFM images we can notice that most of the SNPs were not aggregated, which could be indicator that the outer surface of the particles has negative charge (galacturonic acid), which give electrostatic repulsion force between them, and make another evidence that the SSPS is the shell.

3.6. Rheological measurements

The viscoelastic behaviors of a hydrogel can be determined by the rheological test where the variations of elastic modulus (G′) and viscous modulus (G″) are used to monitor the internal structure changes during its formation where the G′ curve intersected with a G″ curve at the gel point (Yu, Yan, Han, & Huang, 2013; Zhou et al., 2020). As G′ becomes higher than G″, a dominant elastic hydrogel with a crosslinking structure is formed. Here, the viscoelastic differences were further quantified by dynamic rheological measurements of the elastic modulus (G′) and the viscous modulus (G″) as a function of angular frequency (rad/s) (Fig.**6A-F).** Samples with 10% of β-CD concentration showed the G′-G″ crossover around (1 rad/s) and both moduli are very close to each other, and after that the G″ became over the G′, which suggests that the hydrogel acted as an entanglement network and the sample was attending to be viscous rather than elastic (fluid-like). At 15% of the β-CD concentration, both G′ and G″ increased together in a straight line, and their values came close at high frequencies (>1 rad/s), indicating a transition to more gel-like viscoelastic behavior. When the β-CD

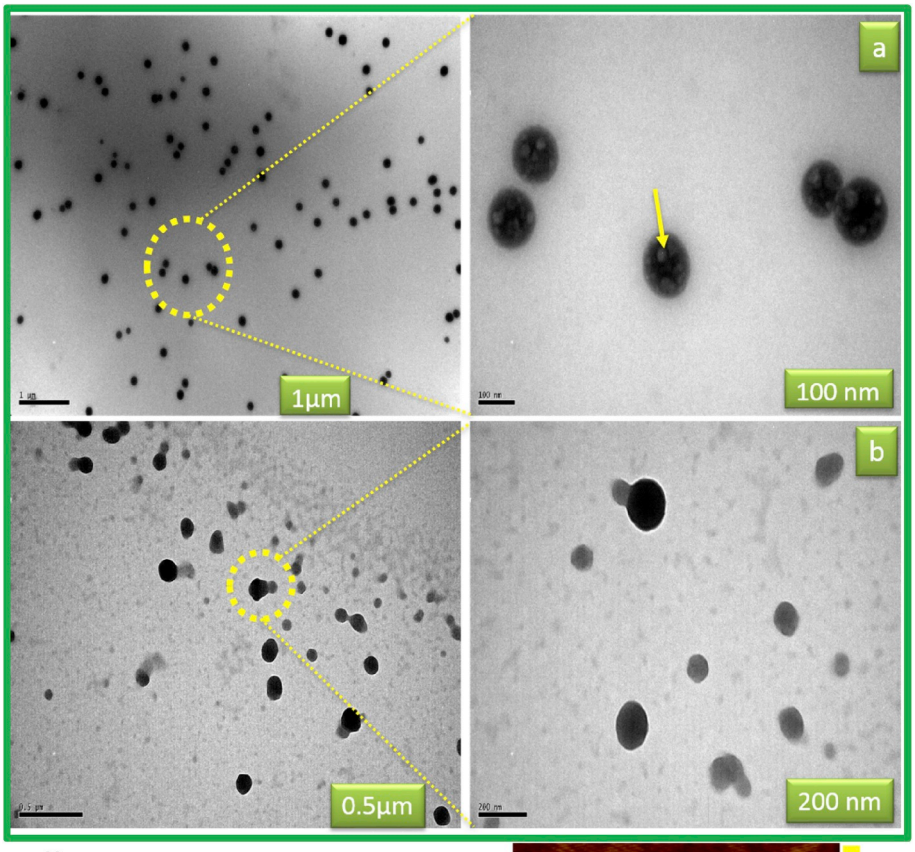

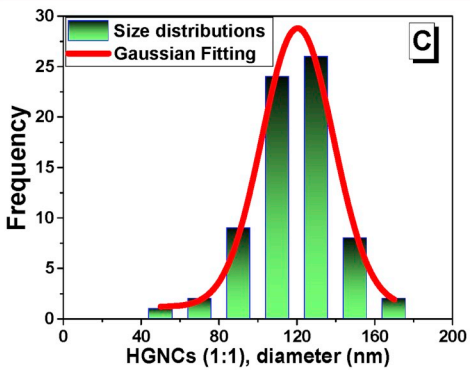

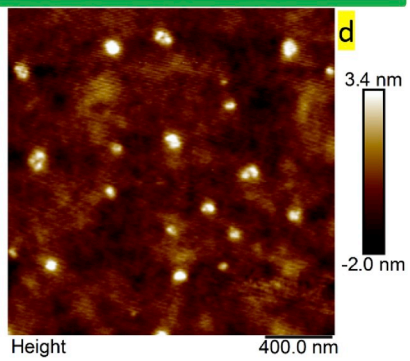

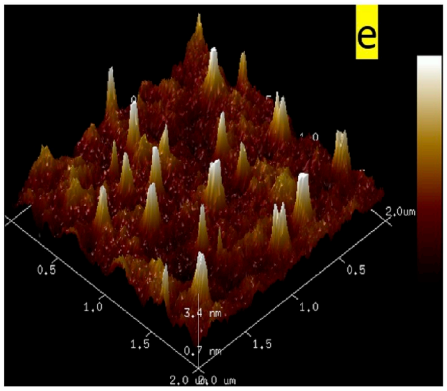

Fig. 5. **a)** displays the TEM image of the HGNCs (1:1) as SNPs. It is obvious that the HGNCs appeared as Nanonetwork structure (the β-CD as multiple small core materials (assigned by yellow arrow) coated by SSPS as single shell material). **b)** HGNCs (1:1)/VE complex **c)** TEM size distribution with Gaussian fitting of the HGNCs (1:1). **d and e)** show the 2-D (in form of white patches) and 3-D (in form of spikes) of AFM images of HGNCs (1:1), respectively. (For interpretation of the references to color in this figure legend, the reader is referred to the Web version of this article.)

concentration was further increased to 20 and 25%, G′ exceeded G″ over the entire angular frequency range established in the examination, indicating that the hydrogel is highly network structured. On the other hand, the strength of the colloidal forces is reflected by tan (δ)= (G″/G′). In both 20 and 25% β-CD concentration have a tan (δ) less than 1, which suggests that the particles are highly associated due to the colloidal forces and sedimentation could occur, while the 10 and 15% β-CD concentration refer to a stable gel system, due to the tan δ is approximately equal 1 (Yu et al., 2013). The effect of β-CD different concentrations with SSPS on the hydrogel viscosity was also investigated, and to evaluate the basic fluid property of the hydrogel different formula, the effect of shear rate on the viscosity was investigated (Fig. 6G). All the

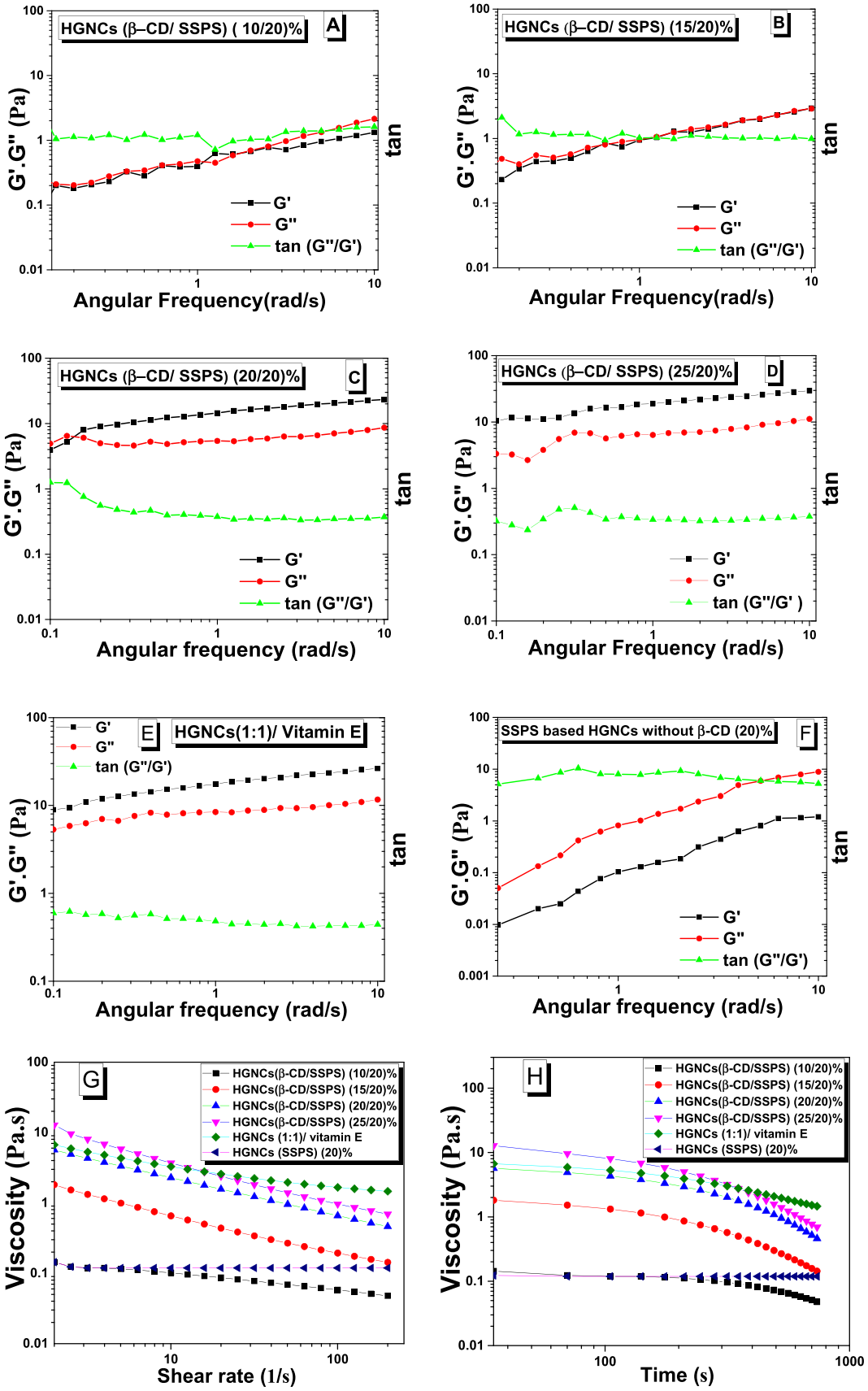

Fig. 6. **(A–D)** The elastic modulus G′ and viscous modulus G″ were plotted logarithmically against angular frequency (0.1 (rad/s), at 25 °C) of the corresponding HGNCs samples **(E)** Flow curve from low to high shear rates (2–200 s^{-1}) **(F)** show a time-dependent change in viscosity.

concentrations exhibited Non-Newtonian behavior or shear-thinning (pseudoplastic) over the entire shear rate range because of the viscosity of samples decreased with increasing the shear rate, and this property supports the sustain drug delivery system of this hydrogel (Bradley et al., 2015). On the other hand, the HGNCs formed by only SSPS (20%) exhibited Newtonian behavior as shown by the independence of the viscosity with increasing the shear stress. Also, the influence of time on the viscosity of all the HGNCs was investigated (Fig. 6H). The characterization of the rheological properties of SSPS based HGNCs without β-CD was also carried out to make sure that the SSPS has low viscosity and can't form the HGNCs alone, so the results showed that the material exhibited viscous than elastic due to the G″ became over the G′ and the tan δ value increases above 1, as shown in (Fig. 6F). Also, we tested the effect of VE inside the HGNCs structure and found by complexing the VE with the HGNCs the G′ slightly increased from 23.30 to 26.05 (Pa) (Fig. 6E). And as reported previously that by increasing the VE from 1.25 to 2.5% at a polymer concentration of 8 wt% gave a 1-fold increase in the storage modulus (G′) (Lee, Ng, Gao, Hedrick, & Yang, 2014). Other researchers tried to enhance the SSPS rheological properties by using monovalent and divalent ions such as (Mg^{+2}, K^{+}, Na^{+}), and they concluded that Mg^{+2} form amore stable and uniform gel network structure than (K^{+} and Na^{+}) as confirmed by G′ and tan (δ). Due to, the Mg^{+2} can reduce the repulsion force between the SSPS chains (S. Wang et al., 2019). Now, incorporation of the β-CD into the SSPS NPs makes the HGNCs a better candidate for biomedical applications.

3.7. Mechanical and adhesive properties

The viscoelastic materials have unique properties, which exhibited viscous and elastic behavior when exposed to compress and loading, therefore we cannot define ideal mechanical characteristics for the hydrogels, because it depends on the site of application. Due to the strong interaction between the β-CD and SSPS in the HGNCs network, our hydrogel has mechanical properties (Fig. 7c). shows the compression strain at (20%) for all samples. The final compression stress increased with increasing β-CD content, being 0.005 MPa (1.58 N), 0.01 MPa (3.13 N), 0.0164 MPa (5.12 N), and 0.025 MPa (7.89 N) from low to high β-CD content, and for (HGNCs (1/1)/VE) and SSPS (20%), being 0.015 MPa (4.89 N) and 0.00036 MPa (0.063 N), respectively. Our results are in accordance with those of (Yuan et al., 2019), who examined the impacts of different kinds of CDs on the texture of the κ-carrageenan (KC)/konjac glucomannan (KGM) compound gels. Also, Liu et al., found that by increasing the SSPS than kudzu and lotus starches the hardness and elasticity of the gel decreased (Liu, Li, Fan, Zhang, & Zhong, 2019). Additionally, Our HGNCs performed as viscoelastic materials under loading with an elastic linear region followed by plastic deformation (relaxation). (Fig. 7d), showed all the HGNCs with superelastic behavior, that the HGNCs with or without VE was able to complete recovery to its native shape when uncompressing, also (Fig. 7a), illustrated the pliability and flexibility of the HGNCs, which could be compressed and released many times without any damage or fracture, which has also been confirmed by doing 5 cycles loading/unloading with 90% strain (Fig. 7e). On the compressive loading-unloading cycle, the area of the hysteresis loop (dissipated energy), were different from each other and enhanced with increasing the amount of β-CD, due to the improved cross-linking degree of the network resulted in increasing the hardness and modulus of elasticity (Young's modulus, Fig. 7f). Also, proved that the β-CD and SSPS macromolecule chains were entangled with the crosslinker (PEGDE) and formed strong chemical crosslink (Dong et al., 2013). Notably, by using the inclusion complex interaction with VE we can notice that the mechanical properites (compression, loading-unloading cycle, hardness, and young's modulus) slightly changed due to the lipids (VE) are not capable to form cohesive substances, especially with polysaccharides. On the other hand, the HGNCs with adhesiveness would be used in biomedical applications, including tissue repair, and bio-glue. It could be adhesive to different solid surfaces by chemical or physical bonds. However, the physical interactions are worth to design multi-purpose and reusable adhesive hydrogels (Yuk, Zhang, Lin, Parada, & Zhao, 2016). To prepare the adhesive hydrogel, SSPS was introduced into the HGNCs formation to improve the balance of cohesion and adhesion (Fig. 1) (Liu et al., 2019). The SSPS contains an amount of soy protein which having essential and acidic amino acids, besides the negative charge from the carboxylic groups (galacturonic acid, 18%) in the main building structure of the SSPS. All these groups can provide physical crosslinking via hydrogen bonding, hydrophobic interaction, metal binding, and other synergistic interactions. The HGNCs driven by SSPS exhibited an excellent adhesive property, which can adhere to the surface of several solids as exposed in (Fig. 7b). This adhesive also may be described by the foundation of (IC) between the β-CD and the hydrophobic protein moieties that are available at the HGNCs surface.

3.8. Swelling behavior

Hydrogels with a uniform nanostructure can hold much water resulting in a higher water capacity (Li et al., 2015; Panja et al., 2016). Our (3 D) HGNCs absorbed water and became transparent hydrogel especially in low concentrations than higher concentrations due to the cross-linking density as appeared in (Fig. 8A). We also can observe in (Fig. 8B) the HGNCs diameter changed after swelling from 20 mm to 35 mm with a 1.5-time increase in the (HGNCs,1/1) as confirmed in the TEM section (de)-swelling, which recorded as 1.4-times increase. The maximum reswelling of the hydrogels after first washing and drying recorded after 24 h. Besides, The HGNCs absorbance exhibited that the swelling increased with decreasing the β-CD content (10%) to SSPS (20%) with water absorbency 2017 ± 11.9 g/g hydrogel. On the other hand, the swelling of the HGNCs with higher β-CD content (25%) showed the lowest swelling property compare to others, which specifies that the entanglement of hydrogel was curbed by β-CD molecules reached to 679 ± 25 g/g hydrogel. Also, the morphology study (pore size) of the hydrogels can confirm these results. Besides, The presence of SSPS polymer chains, as well as the cross-linker (PEGDGE) on the HGNCs structure increased the hydrophilicity of the network. However, the absorbancy decreased by incorporating a high proportion of β-CD inside the network structure because of the steric effect of the β-CD molecules, (Fig. 8C).

3.9. Dynamic light scattering (DLS), zeta potential (ζ), and surface hydrophobicity (H0) measurements

The prepared HGNCs was characterized in aqueous dispersion by dynamic light scattering (DLS; Fig. 9A). The low β-CD content (10%) in the HGNCs with high SSPS content 20% leads to particle dispersions with a multimodal, large size distribution over length scales (Fig. 9A and b). And this corresponds to the multimodal size distribution curve of the SPSS (Fig. 9A, a). The multimodal distribution obtained confirms that there were some aggregates present by the hydrophobic interactions of the SSPS protein. By increasing the β-CD content to SSPS concentration of (10/20), (15/20), (20/20), and (25/20) %, we have obtained uniform particles with narrow size distribution besides, increasing the hydrodynamic diameter (D_h) from 114.2 ± 4 to 134.3 ± 2 and further to 174.3 ± 3 and 202.9 ± 12, respectively. Obviously, the β-CD supports and stabilizes the formation of more uniform structures, and subsequently chemically cross-links the HGNCs as shown in the TEM image. On the other hand, the (HGNCs/VE) complex showed higher nanosized (245 ± 6 nm) than others. The zeta potential (ζ) of the SSPS and HGNCs with and without VE was measured at different pH (3, 7, and 9) with values (−3.3 ± 0.24, −1.2 ± 0.36, and −0.80 ± 0.11 mV) at pH 3, (−10.93 ± 0.757, −9.38 ± 0.45, −8.01 ± 0.40 mV) at pH 7, and (−15.76 ± 0.90, −10.73 ± 0.80, −9.57 ± 0.08) at pH 9 for SSPS, HGNCs, and HGNCs/VE, respectively as shown in (Fig. 9B). We noted that by increasing the pH value the negative charge of SSPS and HGNCs increased dramatically,

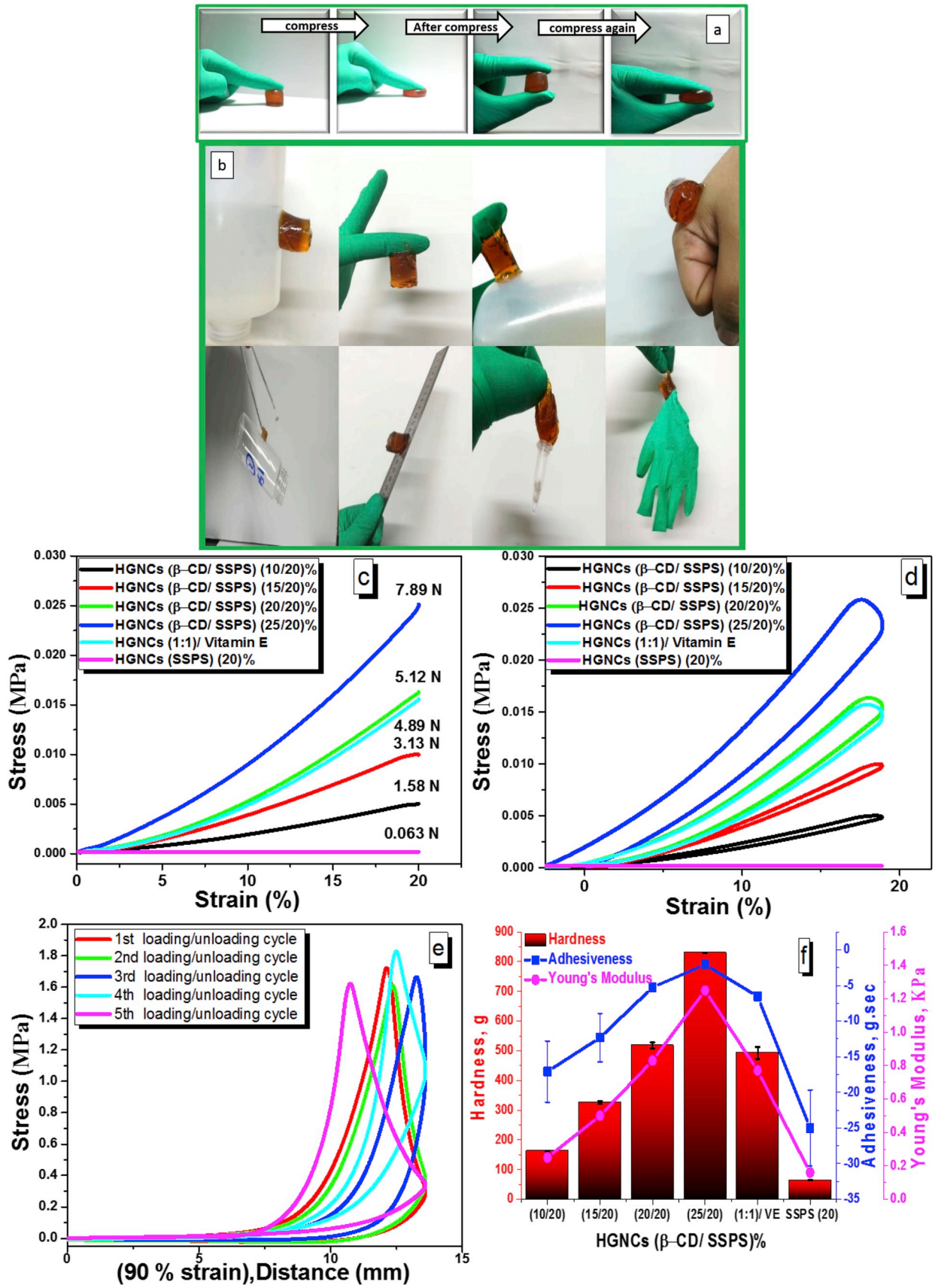

Fig. 7. **(a)** Schematic representation of the compress and release of soft and flexible (β-CD/SSPS) HGNCs **(b)** Adhesion between different adherends and hydrogels, including plastics, human skin, glasses, stainless steel, polypropylene, and rubbers (from left (top) to right (bottom) **(c)** The compressive stress-strain curves at 20% strain **(d)** Compression loading/unloading curves and corresponding stress of HGNCs with a different ratio between β-CD and SSPS **(e)** five loading/unloading cycles on HGNCs (1/1) at 90% strain **(f)** the corresponding Hardness, Adhesiveness, and Elastic modulus (Young's modulus) of the different HGNCs.

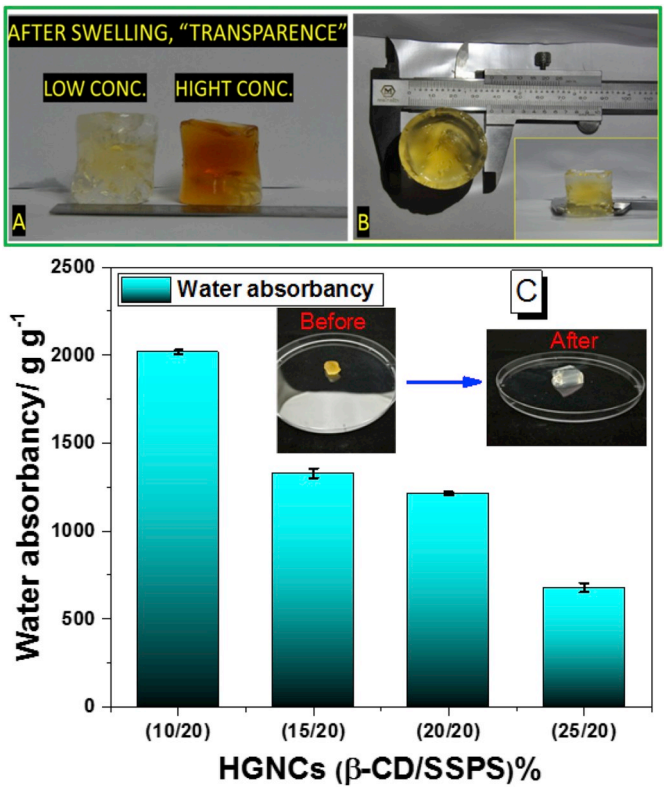

Fig. 8. **(A)** shows the difference between low and high concentrations between the (β-CD/SSPS) ratios **(B)** The diameter of the hydrogel was measured using a caliper. **(C)** Water absorbency of the (β-CD/SSPS) HGNCs in deionized water.

which confirmed that the surface of the gel-coated with the SSPS polysaccharides and the difference between them due to the incorporation of the SSPS chains into the gel network structure. The (ζ) values changed slightly after the VE loaded compare with before loading. However, there was significant size increase with VE uploading, which indicates that the VE was not adsorbed to the surface due to washing the gels with ethanol but entrapped inside the gel structure. The surface hydrophobicity (H0) is an indicator of the wide variety of hydrophobic groups on the surface of different materials like protein (F.-P. Chen, Ou, et al., 2016). Heat treatment of the SSPS during the HGNCs formation resulted in a considerable increase in (H0) of the hydrogel surface, but the extent of increase varied with different β-CD concentrations. The (H0) value of 10 > 15>20 > 25%, manifesting that by increasing the weight ratio between the two polymers the interaction covered some of the hydrophobic groups of soy protein which gave decrease exposure of hydrophobic groups onto the surface, meanwhile the SSPS has highly branched chains some branches still exposed outside and gave some hydrophobicity appeared also in adhesive analysis (Ding et al., 2013). Also, we examined the H0 with the HGNCs (1/1)/VE complex and found small changes in the intensity between them confirming that the SSPS represent the shell and the β-CD is the core with trace of VE molecules on the surface, (Fig. 9C).

3.10. HGNCs polysaccharide hydrolysis

To further confirm the structure of the composites (core and shell), polysaccharide (SSPS) and oligosaccharide (β-CD) hydrolysis were achieved by using pectinase and α-amylase, respectively (Nakamura, Yoshida, Maeda, Furuta, & Corredig, 2004). The hydrolysis of diluted HGNCs dispersion solution with enzymes was done at pH 4.0 and 7.0 for pectinase and α-amylase, respectively at 25 °C, and the DLS measurement was recorded in required real-time. Before the addition of pectinase and α-amylase, the size was 371 ± 11.85 and 176 ± 4.40 nm, respectively (Fig. 10 a, and b). We attributed the large HGNCs size in acidic media than the neutral one due to the assemblage of the NPs by the hydrophobic protein inside the SSPS which confirmed also that the HGNCs has the SSPS as the outer phase (Ding et al., 2013). After the addition of pectinase enzyme, the size started to decrease gradually to reach 75 ± 1.90 nm after 120 min. While, in the case of α-amylase enzyme the size began with 176 ± 4.40 nm and by the degradation time reached to 119 ± 2.12 nm, and suddenly increased to 121 ± 1.90 and 124 ± 2.40 nm after 120 min and this could be happened after the β-CD hydrolysis and the SSPS molecules started to make conglomerates with themselves by electrostatic interaction. From these results, we can imagine that the HGNCs have the SSPS as the outer surface.

3.11. Confocal laser scanning microscopy (CLSM)

The CLSM images of β-CD/VE-IC, uncompressed and compressed HGNCs samples, respectively are showed in (Fig. 11). Firstly, VE in ethanol could be stained by Nile Red, while β-CD and HGNCs could be stained by Nile Blue. The β-CD/VE-IC stained after the (IC) formed, and the (HGNCs/VE) stained as mentioned by swelling technique (section 2.14). The samples incubated with the dyes overnight in a dark place and showed under 633 and 488 nm wavelength laser irradiation, respectively. The β-CD/VE-IC exhibited in the combined channel a fluorescence yellow spots concentrated in the central area of the (IC) under the superimposed channel (Fig. 11C), which could be attributed to the presence of VE inside the β-CD cavities. Furthermore, we have got a confirmed image in the case of uncompressed HGNCs with VE (Fig. 11F), which make sure that the β-CD centered in the middle of the gel as a core and the SSPS covered it as a shell, and we can notice the yellow fluorescence of the VE molecules appeared from the center. Besides, to detect the (IC) inside the HGNCs we compressed it between the microscope slides and noted that the VE found in the center of the β-CD cavity (Fig. 11I), which confirmed our previous results and demonstrated a good HGNCs with flexible network structure that can invite hydrophobic molecules like drugs and vitamins.

3.12. Complexation and dynamic release of VE by/from HGNCs in vitro

Swollen HGNCs do improve in the loading and release of the drugs depend on their swellability degree, nanosized, polymer density, mesh size, and flexibility structure (Münster, Capáková, Fišera, Kuřitka, & Vícha, 2019). Chen et al. prepared a hydrogel electrospun fiber by using chitosan and polyvinyl alcohol (PVA), and they found that the drug release rate of the desferioxamine (DFO) increased by increasing the water content, thus the drug release was over 92.7% after 72 h (H. Chen, Ou, et al., 2016). Since our HGNCs could absorb much water (showed in section 3.8), which could be an effective way to increase the surface area and active the functional cavities of the β-CDs. We used this property to absorb the VE in the aqueous media as a hydrophobic drug model with ethanol as an emulsifier. In this work, VE (25% w/w) diluted with the alcohol and added to the HGNCs in water. The addition of the VE is observed directly from the decrease of transparency through the formation of white cloud. The tubes sealed so that the alcohol would not evaporate and keep the emulsion stable. During the swelling of the HGNCs, the hydrophobic VE molecules go through the hydrogel pours with water and bind to the hydrophobic interior surfaces of covalently embedded β-CD. The effect of varying β-CD/SSPS weight ratios on the VE entrapment efficiency (EE) % and loading capacities (LC)% were calculated and the results showed in Table 1. Herein, we can say that the VE distributed inside the cavities of the β-CDs in the middle of the HGNCs structure and the SSPS covered the molecules as a shell to protect the vitamin and support the slow release property as confirmed in the TEM and CLSM images. Comparing with others, wang et al., prepared hydrogel beads by using (4 wt%) soybean hull polysaccharides and (0.2 M) $CaCl_2$ as a cross linker to encapsulate the isoflavone (hydrophobic compound). The values of (EE) % and (LC) % were 66.90% and 4.67%,

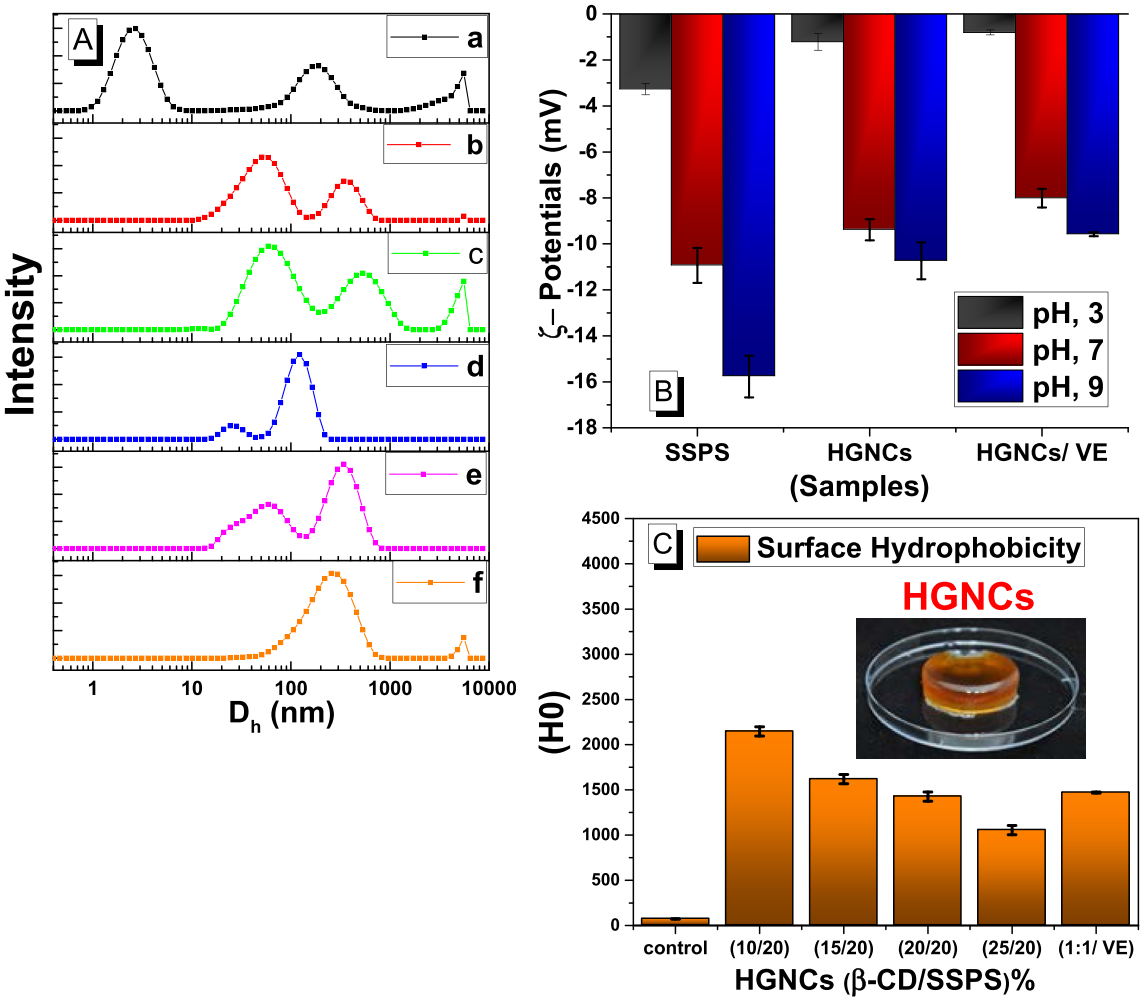

Fig. 9. A) DLS-measurements in aqueous dispersion at 25 °C; size distributions of SSPS **(a)** and HGNCs with different β-CD content 10, 15, 20, 25% (**b, c, d, and e**, respectively) and size distribution of HGNCs/VE complex in aqueous dispersion **(f)**. **B)** ζ potentials of SSPS, HGNCs, and HGNCs/VE complex at different pH values. The Hydrogels was produced with a concentration of 5 mg/mL and sonicated for 1 min. **C)** surface hydrophobicity of HGNCs different concentrations with and without Vitamin E (VE), Each value represents the peak area mean with ±SD.

respectively during 24 h (S. Wang et al., 2020).

Vitamin E dispersed in the glassy HGNCs after drying, and when the polymer network subjected into an aqueous solution, it undergoes a transition from glassy state to a rubbery state. The release mechanism depends on both the characteristics of the polymeric network and the drug. When the polymer and the drug such as (VE) interact via non-covalent interactions (i.e., electrostatic or hydrophobic), the release of such hydrogels depends on the dissociation rate of the drug from the polymer matrix (Vermonden, Censi, & Hennink, 2012). We have investigated the release kinetics of VE from the HGNCs with different β-CD concentrations, and the amount of the release was quantified in the incubation solution. Overall, by increasing the crosslinking between the two polymers resulted in a decreased in VE release rate (Fig. 12). The hydrogel samples with 10% and 15% of β-CD have nearly 51 and 47%, respectively of VE were released within 13 h but after increasing the time to 230 h, the release reached to nearly 94 and 69%, respectively. On the other hand, when the β-CD concentration increased to 20 and 25%, within the first 13 h, only 28 and 24% VE were released, respectively and after 230 h the release became 48 and 44%, respectively. This mechanism of release agreed with Chen et al. that they formed photo cross-linked gelatin hydrogel (Gelma) for releasing the (DFO) drug and found that the Gelma exhibited swelling burst release until 16 h and turned to slow emotion of release after 48 h in PBS at 37 °C (Hao Chen, Ou, et al., 2016). And to be sure that the swelling property was responsible for the controlled release of the VE not the diffusion or erosion of the gel, the VE release profiles were analyzed using mathematical model recognized in the previous hydrogel drug release studies (Peppas, 2014). The details showed in the supporting information with (Figs. S2 and S3).

3.13. *In vivo VE bioavailability and pharmacokinetics study in rats*

Recently, it is reported that the SSPS can promote the absorption of some chemical drugs (Lu et al., 2019). Thus, we speculated that SSPS with β-CD as HGNCs may improve the absorption of VE in rats due to the bioavailability of VE is limited (Duhem, Danhier, & Preat, 2014). The overall bioavailability (BA) of VE can be defined as the fraction that eventually reaches the systemic circulation in an active form, which can be described by the following expression: (BA) = (B) × (A) × (T). Now, (B) is the fraction of VE solubilized in the mixed micelle phase (bioaccessibility), (A) is the fraction of VE absorbed by the epithelium cells (absorption), and (T) is the fraction of the VE in a bioactive form after passage through the epithelium cells (transformation) (Duhem et al., 2014; Yang, Xiao, & McClements, 2017). In our in vivo study the overall relative bioavailability (BA)% was obtained after the HGNCs (different compositions) orally administrated. The results are summarized in Table 2. In general, the increase in C_{max} indicates that our HGNCs was effectively enhancing the absorption of VE. The HGNCs with low β-CD

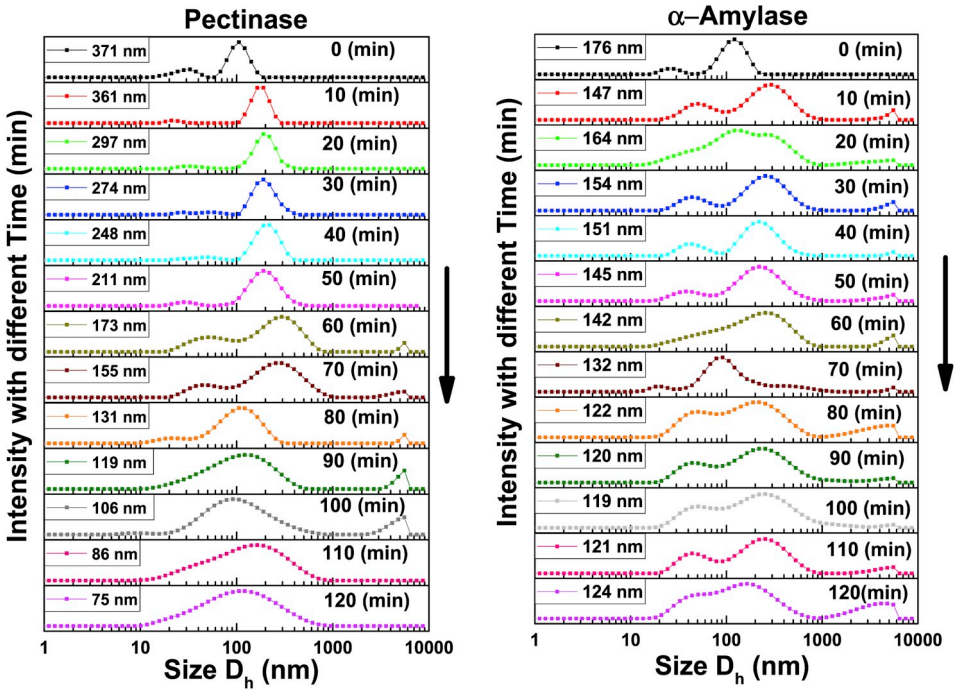

Fig. 10. a) Real-time DLS result of the (β-CD/SSPS) HGNCs during the polysaccharide hydrolysis by pectinase at pH 4.0 at different times **b)** Real-time DLS result of the (β-CD/SSPS) HGNCs during the polysaccharide hydrolysis by α-Amylase at pH 7 at different times.

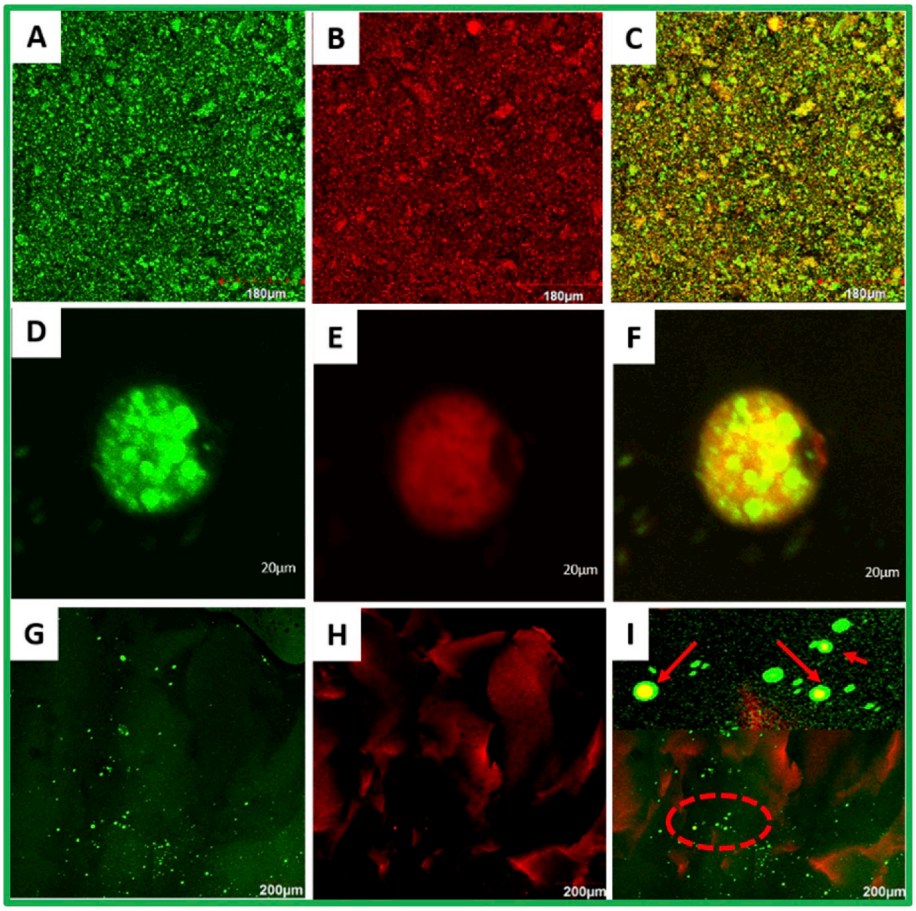

Fig. 11. CLSM images with three channels (green, red, and combined): (A–C) β-CD/VE- IC, (D–F) Uncompressed HGNCs/VE complex, (G–I) Compressed HGNCs/VE showed the (IC) under 633 and 488 nm wavelength superimposed laser channels. (For interpretation of the references to color in this figure legend, the reader is referred to the Web version of this article.)

Table 1
Represented the Encapsulation Efficiency (**EE**)% and Loading Capacity (**LC**)% of the (β-CD/SSPS)-HGNCs samples. Each value represents mean ± SD (n = 3).

(HGNCs) (%)	(EE) %	(LC) %
(10/20)	79.10 ± 0.67	16.04 ± 0.27
(15/20)	67.24 ± 0.56	14.39 ± 1.31
(20/20)	46.99 ± 0.39	8.52 ± 0.007
(25/20)	37.22 ± 0.32	6.33 ± 0.007

content (10 and 15%) with higher SSPS concentration (20%) had a higher $AUC_{0-\infty}$ (106.18 and 87.53 μg h/mL, respectively, which proved a 7.5 and 6.2- fold increase in the bioavailability) than the free VE suspension. While, the HGNCs with β-CD content (20 and 25%) had a higher $AUC_{0-\infty}$ (65.78 and 33.75 μg h/mL, respectively, which proved a 4.6 and 2.4- fold increase in the bioavailability) (Fig. 13). Our results are higher than other researchers like Song et al. that they exposed the sustained release of VE encapsulated by Ca-pectinate using an in vivo animal study. And the area under the curve (AUC) for the micro-encapsulated VE increased by about 118% when compared to free VE (Y.-B. Song, Lee, & Lee, 2009). Our outcomes suggested that the SSPS as a shell material is effective at increasing the bioavailability of VE, which has important implications for designing effective HGNCs delivery system for the hydrophobic drugs. The high swelling property was applied to develop the intestinal retention system that can remain the HGNCs in the digestive system due to its large size after swelling (3D structure). Moreover, as the SSPS is anionic polysaccharide it can protect the HGNCs from the release in stomach due to the low network swelling in the acidic media (pH 1–3), the data is not shown (F.-P. Chen, Ou, et al., 2016), besides it can protects the VE from the harsh conditions and enzymes (gastric lipases and proteases). As a result, at pH 6.8, the network became ionized with a higher swelling resulted in increased VE release than in the gastric fluid. And due to the high surface area, high polarity (SSPS), and the increased volume (3D), the HGNCs were able to stick to the intestinal gut wall mechanically (mucoadhesive) and deliver the incorporated VE directly to the gut wall. On the other hand, we attributed the differences in bioavailability between the HGNCs formations due to the variations of interaction between the two biopolymers as confirmed in the SEM morphology and in vitro release study. Also, Sun et al. found that by increasing the crosslinking degree between the two polymers, the hydrogel became more stiffness and the diffusion and release of nutrients through the porous structure decreased (Sun et al., 2018). Moreover, as the β-CD cannot be degraded in the small

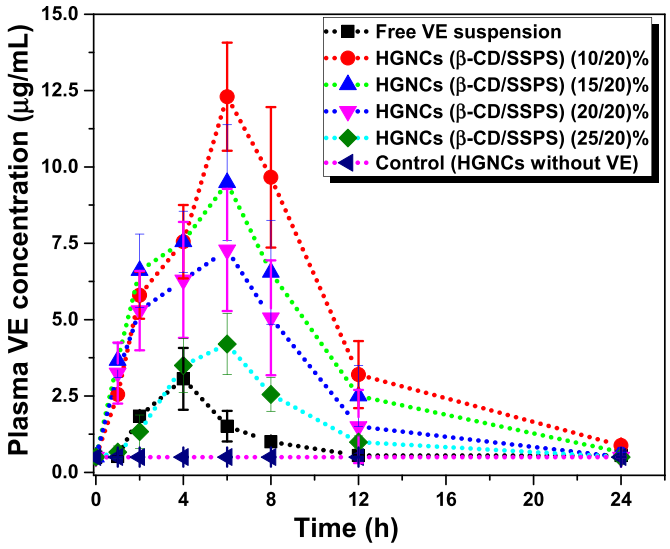

Fig. 13. Plasma concentration (μg mL^{-1}) of Vitamin E (VE) *versus* time (h) after oral administration as a free suspension and complexed with HGNCs different compositions. Each value represents mean ± SD (n = 3).

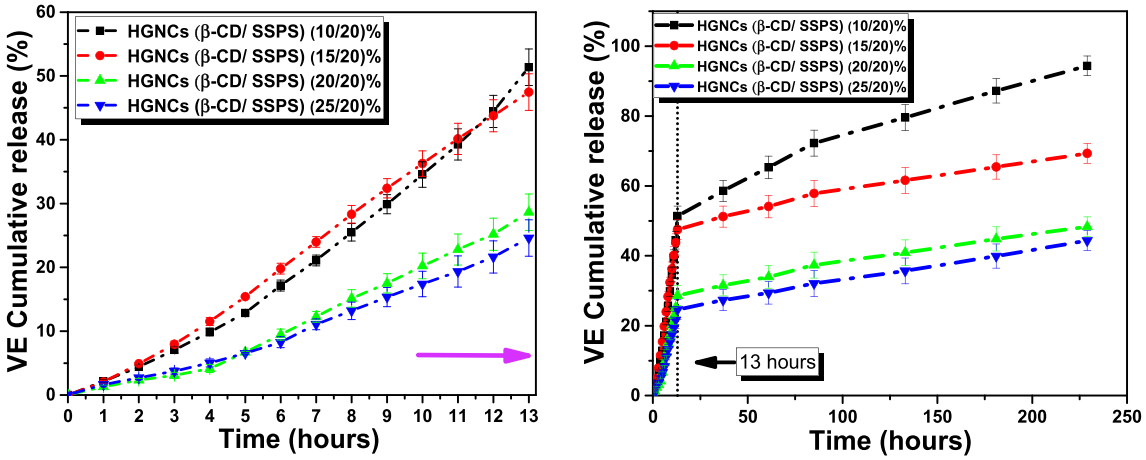

Fig. 12. In vitro kinetic release profiles of VE from (β-CD/SSPS) HGNCs in 5 mM PBS (pH 7.4, containing 5 mg/mL Tween 20). Each data point is the means and standard deviations (n = 3).

Table 2
Pharmacokinetics (PK) Parameters of free VE suspension and HGNCs/VE different composites (%) administrated orally in rats [a].

Samples (%)	C_{max} (μg/mL)	T_{max} (h)	K e (h^{-1})	AUC_{0-t} (μg h/mL)	$AUC_{0-\infty}$ (μg h/mL)	BA (%)
VE suspension	3.06 ± 1.01	4	0.094 ± 0.01	13.74 ± 0.54	14.05	–
(10/20)	12.30 ± 1.77	6	0.143 ± 0.02	105.83 ± 8.20	106.18	755.72
(15/20)	9.48 ± 1.90	6	0.147 ± 0.02	87.40 ± 3.60	87.54	623.06
(20/20)	7.27 ± 2.00	6	0.150 ± 0.03	65.64 ± 3.66	65.78	468.18
(25/20)	4.20 ± 1.00	6	0.151 ± 0.03	33.68 ± 2.55	33.75	240.21

[a] Each value represents mean ± SD (n = 3). C_{max}: maximum plasma concentration; T_{max}: time to reach maximum plasma concentration; Ke: the elimination rate constant; AUC: area under plasma concentration−time curve; BA (%) the percent relative bioavailability. Data were collected using non-compartmental analysis.

intestine the VE release is affected mostly by the swelling degree and the network flexibility. So, we can advise here using a high amount of β-CD with SSPS to release other specific bioactive components to the colon, where colonic fermentation destroys the β-CD (Hedges, 2009). Finally, our in vivo study may provide some strategies to enhance the overall oral bioavailability of hydrophobic ingredients.

4. Conclusions

In summary, this work aimed to evaluate and exploit the application potential of the HGNCs as dynamic carriers and drug control release. For this, a high amount of β-CD and SSPS were selected to act as core-shell bionanomaterials, respectively to host the VE as a model of hydrophobic compounds. Due to, its applications in nutrition is still limited due to the low aqueous solubility, low bioavailability, and high sensitivity. The core-shell structure confirmed by surface hydrophobicity (H0), TEM, CLSM, adhesiveness, zeta potential, enzyme hydrolysis, and XRD. The whole preparation procedure is introduced in one step. Our hydrogels are prepared in alkaline aqueous solution with PEGDGE as suspension cross-linking by incorporating the β-CD domains in the polymer backbone of SSPS via covalent (ether bond) and noncovalent bonding between the hydroxyl (-OH), Amine (-NH2), and Carboxyl (-COO) groups of SSPS and (-OH) groups of the β-CD units. Furthermore, their several nanometers can be controlled by β-CD content, as an increasing of β-CD concentration in the reaction mixture (from 10 to 25%), leads to an increase of size (from 114.2 to 202.9 nm, respectively) and the hardness (from 0.005 to 0.025 MPa) under 20% strain. Besides, Integrating the SSPS (as a shell), and its small hydrophobic protein with β-CD yielded a HGNCs with high swelling, prolonged-release, elasticity, shear-thinning behavior, surface hydrophobicity (H0), and adhesiveness. Also, the SSPS enabled the HGNCs to completely recover its shape when compressed by 90% strain with (1.8 MPa) strength due to its controllable and layered structure as skin. Overall, after taking the in vitro and in vivo studies into consideration, it can be concluded that our HGNCs would be used for delivering VE to its favorable absorption site (small intestine) with 7.5-fold increase than free VE suspension.

Declaration of competing interest

There is no conflict of interests among authors.

CRediT authorship contribution statement

Mohamed Eid: Writing - original draft, Methodology, Conceptualization, Visualization, Formal analysis, Validation, Investigation. **Remah Sobhy:** Writing - original draft, Formal analysis, Methodology. **Peiyuan Zhou:** Resources, Software. **Xianling Wei:** Investigation, Data curation. **Di Wu:** Resources, Software, Investigation. **Bin Li:** Supervision, Project administration, Funding acquisition.

Acknowledgments

The authors gratefully acknowledge National Key R&D Program of China (Program No. 2017YFD0400205) & National Natural Science Foundation of China (Grant No. 31772015), and the Chinese Scholarships Council (CSC) Foundation (No. 2016GXY902) for their financial support.

Appendix A. Supplementary data

Supplementary data to this article can be found online at https://doi.org/10.1016/j.foodhyd.2020.105751.

References

Alizadeh-Pasdar, N., & Li-Chan, E. C. Y. (2000). Comparison of protein surface hydrophobicity measured at various pH values using three different fluorescent probes. *Journal of Agricultural and Food Chemistry, 48*(2), 328–334.

Aytac, Z., Kusku, S. I., Durgun, E., & Uyar, T. (2016). Quercetin/beta-cyclodextrin inclusion complex embedded nanofibres: Slow release and high solubility. *Food Chemistry, 197*(Pt A), 864–871.

Aytac, Z., & Uyar, T. (2017). Core-shell nanofibers of curcumin/cyclodextrin inclusion complex and polylactic acid: Enhanced water solubility and slow release of curcumin. *International Journal of Pharmaceutics, 518*(1–2), 177–184.

Becher, T. B., Mendonca, M. C. P., de Farias, M. A., Portugal, R. V., de Jesus, M. B., & Ornelas, C. (2018). Soft nanohydrogels based on laponite nanodiscs: A versatile drug delivery platform for theranostics and drug cocktails. *ACS Applied Materials & Interfaces, 10*(26), 21891–21900.

Bradley, P., Gordon, N. C., Walker, T. M., Dunn, L., Heys, S., Huang, B., et al. (2015). Rapid antibiotic-resistance predictions from genome sequence data for Staphylococcus aureus and Mycobacterium tuberculosis. *Nature Communications, 6*, 10063.

Butt, A., Jabeen, S., Nisar, N., Islam, A., Gull, N., Iqbal, S. S., et al. (2019). Controlled release of cephradine by biopolymers based target specific crosslinked hydrogels. *International Journal of Biological Macromolecules, 121*, 104–112.

Cassano, R., Trombino, S., Muzzalupo, R., Tavano, L., & Picci, N. (2009). A novel dextran hydrogel linking trans-ferulic acid for the stabilization and transdermal delivery of vitamin E. *European Journal of Pharmaceutics and Biopharmaceutics, 72*(1), 232–238.

Celebioglu, A., & Uyar, T. (2017). Antioxidant vitamin E/cyclodextrin inclusion complex electrospun nanofibers: Enhanced water solubility, prolonged shelf life, and photostability of vitamin E. *Journal of Agricultural and Food Chemistry, 65*(26), 5404–5412.

Chen, H., Guo, L., Wicks, J., Ling, C., Zhao, X., Yan, Y., et al. (2016a). Quickly promoting angiogenesis by using a DFO-loaded photo-crosslinked gelatin hydrogel for diabetic skin regeneration. *Journal of Materials Chemistry B, 4*(21), 3770–3781.

Chen, H., Jia, P., Kang, H., Zhang, H. B., Liu, Y., Yang, P. L., et al. (2016b). Upregulating Hif-1 by hydrogel nanofibrous scaffolds for rapidly recruiting angiogenesis relative cells in diabetic wound. *Advanced Healthcare Materials, 5*(8), 907–918.

Chen, X., Lee, D. S., Zhu, X., & Yam, K. L. (2012). Release kinetics of tocopherol and quercetin from binary antioxidant controlled-release packaging films. *Journal of Agricultural and Food Chemistry, 60*(13), 3492–3497.

Chen, F. P., Ou, S. Y., Chen, Z., & Tang, C. H. (2017). Soy soluble polysaccharide as a nanocarrier for curcumin. *Journal of Agricultural and Food Chemistry, 65*(8), 1707–1714.

Chen, F.-P., Ou, S.-Y., & Tang, C.-H. (2016c). Core-shell soy protein-soy polysaccharide complex (Nano)particles as carriers for improved stability and sustained release of curcumin. *Journal of Agricultural and Food Chemistry, 64*(24), 5053–5059.

Chithrani, B. D., Ghazani, A. A., & Chan, W. C. W. (2006). Determining the size and shape dependence of gold nanoparticle uptake into mammalian cells. *Nano Letters, 6*(4), 662–668.

Chivero, P., Gohtani, S., Ikeda, S., & Nakamura, A. (2014). The structure of soy soluble polysaccharide in aqueous solution. *Food Hydrocolloids, 35*, 279–286.

Ding, X., & Yao, P. (2013). Soy protein/soy polysaccharide complex nanogels: Folic acid loading, protection, and controlled delivery. *Langmuir, 29*(27), 8636–8644.

Dong, W., Huang, C., Wang, Y., Sun, Y., Ma, P., & Chen, M. (2013). Superior mechanical properties of double-network hydrogels reinforced by carbon nanotubes without organic modification. *International Journal of Molecular Sciences, 14*(11), 22380–22394.

Duhem, N., Danhier, F., & Preat, V. (2014). Vitamin E-based nanomedicines for anti-cancer drug delivery. *Journal of Controlled Release, 182*, 33–44.

Faradilla, R. H. F., Lee, G., Sivakumar, P., Stenzel, M., & Arcot, J. (2019). Effect of polyethylene glycol (PEG) molecular weight and nanofillers on the properties of banana pseudostem nanocellulose films. *Carbohydrate Polymers, 205*, 330–339.

Hedges, A. (2009). Chapter 22 - cyclodextrins: Properties and applications. In J. BeMiller, & R. Whistler (Eds.), *Starch* (3rd ed., pp. 833–851). San Diego: Academic Press.

Hosny, K. M., Mosli, H. A., & Hassan, A. H. (2015). Soy polysaccharide as a novel superdisintegrant in sildenafil citrate sublingual tablets: Preparation, characterization, and in vivo evaluation. *Drug Design, Development and Therapy, 9*, 465–472.

Hussain, C. M., & Mishra, A. K. (2018). *Nanotechnology in environmental science, 2 volumes* (Vol. 1). John Wiley & Sons.

Jiang, M., Hong, Y., Gu, Z., Cheng, L., Li, Z., & Li, C. (2019). Preparation of a starch-based carrier for oral delivery of Vitamin E to the small intestine. *Food Hydrocolloids, 91*, 26–33.

Jokerst, J. V., Lobovkina, T., Zare, R. N., & Gambhir, S. S. (2011). Nanoparticle PEGylation for imaging and therapy. *Nanomedicine, 6*(4), 715–728.

Kaur, K., & Jindal, R. (2019). Comparative study on the behaviour of Chitosan-Gelatin based Hydrogel and nanocomposite ion exchanger synthesized under microwave conditions towards photocatalytic removal of cationic dyes. *Carbohydrate Polymers, 207*, 398–410.

Kono, H., Onishi, K., & Nakamura, T. (2013). Characterization and bisphenol A adsorption capacity of beta-cyclodextrin-carboxymethylcellulose-based hydrogels. *Carbohydrate Polymers, 98*(1), 784–792.

Koontz, J. L., Marcy, J. E., O'Keefe, S. F., & Duncan, S. E. (2009). Cyclodextrin inclusion complex formation and solid-state characterization of the natural antioxidants alpha-tocopherol and quercetin. *Journal of Agricultural and Food Chemistry, 57*(4), 1162–1171.

Lee, A. L. Z., Ng, V. W. L., Gao, S., Hedrick, J. L., & Yang, Y. Y. (2014). Injectable hydrogels from triblock copolymers of vitamin E-functionalized polycarbonate and

poly(ethylene glycol) for subcutaneous delivery of antibodies for cancer therapy. *Advanced Functional Materials, 24*(11), 1538–1550.
Li, J., Su, Z., Xu, H., Ma, X., Yin, J., & Jiang, X. (2015). Supramolecular networks of hyperbranched poly(ether amine) (hPEA) nanogel/chitosan (CS) for the selective adsorption and separation of guest molecules. *Macromolecules, 48*(7), 2022–2029.
Liu, D., Li, Z., Fan, Z., Zhang, X., & Zhong, G. (2019). Effect of soybean soluble polysaccharide on the pasting, gels, and rheological properties of kudzu and lotus starches. *Food Hydrocolloids, 89*, 443–452.
Lu, Y., Zhao, A., Wu, Y., Zhao, Y., & Yang, X. (2019). Soybean soluble polysaccharides enhance bioavailability of genistein and its prevention against obesity and metabolic syndrome of mice with chronic high fat consumption. *Food & function, 10*(7), 4153–4165.
Michalska, P., Wojnicz, A., Ruiz-Nuno, A., Abril, S., Buendia, I., & Leon, R. (2017). Inclusion complex of ITH12674 with 2-hydroxypropyl-beta-cyclodextrin: Preparation, physical characterization and pharmacological effect. *Carbohydrate Polymers, 157*, 94–104.
Mumper, R. J., Huffman, A. S., Puolakkainen, P. A., Bouchard, L. S., & Gombotz, W. R. (1994). Calcium-alginate beads for the oral delivery of transforming growth factor-β1 (TGF-β1): Stabilization of TGF-β1 by the addition of polyacrylic acid within acid-treated beads. *Journal of Controlled Release, 30*(3), 241–251.
Münster, L., Capáková, Z., Fišera, M., Kuřitka, I., & Vícha, J. (2019). Biocompatible dialdehyde cellulose/poly(vinyl alcohol) hydrogels with tunable properties. *Carbohydrate Polymers, 218*, 333–342.
Nakamura, A., Furuta, H., Maeda, H., Takao, T., & Nagamatsu, Y. (2002). Structural studies by stepwise enzymatic degradation of the main backbone of soybean soluble polysaccharides consisting of galacturonan and rhamnogalacturonan. *Bioscience Biotechnology and Biochemistry, 66*(6), 1301–1313.
Nakamura, A., Yoshida, R., Maeda, H., Furuta, H., & Corredig, M. (2004). Study of the role of the carbohydrate and protein moieties of soy soluble polysaccharides in their emulsifying properties. *Journal of Agricultural and Food Chemistry, 52*(17), 5506–5512.
Olad, A., Doustdar, F., & Gharekhani, H. (2018). Starch-based semi-IPN hydrogel nanocomposite integrated with clinoptilolite: Preparation and swelling kinetic study. *Carbohydrate Polymers, 200*, 516–528.
Panja, S., Dey, G., Bharti, R., Mandal, P., Mandal, M., & Chattopadhyay, S. (2016). Metal ion ornamented ultrafast light-sensitive nanogel for potential in vivo cancer therapy. *Chemistry of Materials, 28*(23), 8598–8610.
Peppas, N. A. (2014). 1. Commentary on an exponential model for the analysis of drug delivery: Original research article: A simple equation for description of solute release: I II. Fickian and non-fickian release from non-swellable devices in the form of slabs, spheres, cylinders or discs, 1987. *Journal of Controlled Release : Official Journal of the Controlled Release Society, 190*, 31–32.
Rodriguez, R., Alvarez-Lorenzo, C., & Concheiro, A. (2003). Cationic cellulose hydrogels: Kinetics of the cross-linking process and characterization as pH-/ion-sensitive drug delivery systems. *Journal of Controlled Release, 86*(2–3), 253–265.
Salarbashi, D., Bazeli, J., & Tafaghodi, M. (2019). Environment-friendly green composites based on soluble soybean polysaccharide: A review. *International Journal of Biological Macromolecules, 122*, 216–223.
Salarbashi, D., Tafaghodi, M., & Bazzaz, B. S. F. (2018). Soluble soybean polysaccharide/TiO2 bionanocomposite film for food application. *Carbohydrate Polymers, 186*, 384–393.
Salvekar, A. V., Huang, W. M., Xiao, R., Wong, Y. S., Venkatrarnan, S. S., Tay, K. H., et al. (2017). Water-responsive shape recovery induced buckling in biodegradable photo-cross-linked poly(ethylene glycol) (PEG) hydrogel. *Accounts of Chemical Research, 50*(2), 141–150.
Saunders, B. R., & Vincent, B. (1999). Microgel particles as model colloids: Theory, properties and applications. *Advances in Colloid and Interface Science, 80*(1), 1–25.
Shaili, T., Abdorreza, M. N., & Fariborz, N. (2015). Functional, thermal, and antimicrobial properties of soluble soybean polysaccharide biocomposites reinforced by nano TiO2. *Carbohydrate Polymers, 134*, 726–731.
Shi, Y., Xiong, D., Liu, Y., Wang, N., & Zhao, X. (2016). Swelling, mechanical and friction properties of PVA/PVP hydrogels after swelling in osmotic pressure solution. *Materials Science & Engineering C-Materials for Biological Applications, 65*, 172–180.
Song, L. X., Bai, L., Xu, X. M., He, J., & Pan, S. Z. (2009a). Inclusion complexation, encapsulation interaction and inclusion number in cyclodextrin chemistry. *Coordination Chemistry Reviews, 253*(9–10), 1276–1284.
Song, Y.-B., Lee, J.-S., & Lee, H. G. (2009b). α-Tocopherol-loaded Ca-pectinate microcapsules: Optimization, in vitro release, and bioavailability. *Colloids and Surfaces B: Biointerfaces, 73*(2), 394–398.
Sun, X., Zhang, H., He, J., Cheng, R., Cao, Y., Che, K., et al. (2018). Adjustable hardness of hydrogel for promoting vascularization and maintaining stemness of stem cells in skin flap regeneration. *Applied Materials Today, 13*, 54–63.
Trindade, G. G. G., Thrivikraman, G., Menezes, P. P., Franca, C. M., Lima, B. S., Carvalho, Y. M. B. G., et al. (2019). Carvacrol/beta-cyclodextrin inclusion complex inhibits cell proliferation and migration of prostate cancer cells. *Food and Chemical Toxicology : An International Journal Published for the British Industrial Biological Research Association, 125*, 198–209.
Veiga, M. D., Merino, M., Fernandez, D., & Lozano, R. (2002). Characterization of some cyclodextrin derivatives by thermal analysis. *Journal of Thermal Analysis and Calorimetry, 68*(2), 511–516.
Vermonden, T., Censi, R., & Hennink, W. E. (2012). Hydrogels for protein delivery. *Chem Rev, 112*(5), 2853–2888.
Wang, P.-P., Luo, Z.-G., & Peng, X.-C. (2018a). Encapsulation of vitamin E and soy isoflavone using spiral dextrin: Comparative structural characterization, release kinetics, and antioxidant capacity during simulated gastrointestinal tract. *Journal of Agricultural and Food Chemistry, 66*(40), 10598–10607.
Wang, S., Shao, G., Yang, J., Liu, J., Wang, J., Zhao, H., et al. (2020). The production of gel beads of soybean hull polysaccharides loaded with soy isoflavone and their pH-dependent release. *Food Chemistry, 313*, 126095.
Wang, Y., Yang, N., Wang, D., He, Y., Chen, L., & Zhao, Y. (2018b). Poly (MAH-beta-cyclodextrin-co-NIPAAm) hydrogels with drug hosting and thermo/pH-sensitive for controlled drug release. *Polymer Degradation and Stability, 147*, 123–131.
Wang, S., Zhao, L., Li, Q., Liu, C., Han, J., Zhu, L., et al. (2019). Impact of Mg2+, K+, and Na+ on rheological properties and chain conformation of soy hull soluble polysaccharide. *Food Hydrocolloids, 92*, 218–227.
Wu, L., Dou, Y., Lin, K., Zhai, W., Cui, W., & Chang, J. (2011). Hierarchically structured nanocrystalline hydroxyapatite assembled hollow fibers as a promising protein delivery system. *Chemical Communications, 47*(42), 11674–11676.
Xiong, W., Wang, Y., Zhang, C., Wan, J., Shah, B. R., Pei, Y., et al. (2016). High intensity ultrasound modified ovalbumin: Structure, interface and gelation properties. *Ultrasonics Sonochemistry, 31*, 302–309.
Yang, Y., Xiao, H., & McClements, D. J. (2017). Impact of lipid phase on the bioavailability of vitamin E in emulsion-based delivery systems: Relative importance of bioaccessibility, absorption, and transformation. *Journal of Agricultural and Food Chemistry, 65*(19), 3946–3955.
Yuan, C., Xu, D., Cui, B., & Wang, Y. (2019). Gelation of κ-carrageenan/Konjac glucommanan compound gel: Effect of cyclodextrins. *Food Hydrocolloids, 87*, 158–164.
Yuk, H., Zhang, T., Lin, S., Parada, G. A., & Zhao, X. (2016). Tough bonding of hydrogels to diverse non-porous surfaces. *Nature Materials, 15*(2), 190.
Yu, G., Yan, X., Han, C., & Huang, F. (2013). Characterization of supramolecular gels. *Chemical Society Reviews, 42*(16), 6697–6722.
Zhang, Y., Huo, M., Zhou, J., & Xie, S. (2010). PKSolver: An add-in program for pharmacokinetic and pharmacodynamic data analysis in Microsoft Excel. *Computer Methods and Programs in Biomedicine, 99*(3), 306–314.
Zhao, J., Wang, Y. C., Ma, Y. Y., Liu, Y. Y., Yan, B. B., & Wang, L. L. (2019). Smart nanocarrier based on PEGylated hyaluronic acid for deacetyl mycoepoxydience: High stability with enhanced bioavailability and efficiency. *Carbohydrate Polymers, 203*, 356–368.
Zhou, P., Eid, M., Xiong, W., Ren, C., Ai, T., Deng, Z., et al. (2020). Comparative study between cold and hot water extracted polysaccharides from Plantago ovata seed husk by using rheological methods. *Food Hydrocolloids, 101*, 105465.
Zhu, X., Lee, D. S., & Yam, K. L. (2012). Release property and antioxidant effectiveness of tocopherol-incorporated LDPE/PP blend films. *Food Additives & Contaminants: Part A, 29*(3), 461–468.